UNIVERSITY OF CAMBRIDGE
Department of Engineering

Rainfall-runoff Processes in Urban Environments

MEng Final Project 2018

Division D

Author Name: Erind Maho

Supervisor: Dr. Dongfang Liang

Date: 30/05/2018

I hereby declare that, except where specifically indicated, the work submitted herein is my own original work.

Signed ______________________________ *date* ______________________________

MEng Final Project 2018
Rainfall-runoff processes in urban environments
Erind Maho, Trinity College

Technical Abstract

Changing precipitation patterns, ageing drainage infrastructure and rapid urbanisation demand for a better understanding of rainfall-runoff processes and the design of flood-proof urban systems. Deadly floods are becoming more and more frequent, causing substantial damage in densely populated areas. There have been numerous case studies on flooding in specific urban areas and how these can be prevented. However, it is unclear how these results can be generalised and there is little literature on how urban characteristics affect flooding. Urban environments are highly complex and it is likely that the flow due to rainfall is affected by numerous urban parameters. Therefore, the main focus of this project was to develop a parametrised approach to gain a better understanding of the impact of urban characteristics on rainfall-runoff processes.

The hydrodynamical model used in this study uses a Total Variation Diminishing MacCormack numerical scheme to solve two-dimensional shallow water equations, which describes the evolution of an incompressible fluid in response to gravity, bed friction and inertia. Initially, the model was validated against published results. Results from Bruwier *et al.* (2017) were reproduced by applying a steady inflow of water across realistic urban layouts and recording the resulting water depths at steady state. Generally, the results showed good agreement, confirming the capability of our model in simulating prescribed water flow over realistic urban layouts.

A kinematic surface runoff model developed by Henderson & Wooding (1964) served as basis for the derivation of analytical relationships describing the hydrological response of a rough, impermeable plane under uniform rainfall. Results from computational simulations on a sloping plane under different combinations of slope and rainfall intensity showed good agreement with the analytical solutions, confirming the capability of our model to predict overland flow over impermeable sloping planes under uniform, constant rainfall of a finite duration.

Next, dimensional analysis was exploited in the examination of S-curve normalisation theory. Simulations were first conducted on a realistic urban layout under different

combinations of slope and rainfall intensity and the resulting hydrographs at the outlet recorded. The dimensionless hydrographs derived using a properly-constructed dimensionless time collapsed to a single *S*-curve for all combinations, confirming that the derived dimensionless *S*-curve is only a function of urban characteristics. This allowed for the use of a dimensionless time of concentration t^*_{70} to characterise the time-scale of the *S*-curve rise and rainfall-runoff response, as a result.

The *S*-curve normalisation theory paved the way for the final stage of the project, a parametric urban runoff study. High performance computing and parallel processing enabled the simulation and processing of 2,994 rainfall-runoff processes. Results were analysed using a multiple linear regression model, which quantified the sensitivity of t^*_{70} to 12 urban parameters. The most influential factors were found to be Manning roughness coefficient n and building coverage, followed by street length, building side setback, parcel area and to a lesser extent, street orientation and curvature. Investigation of the relationships between t^*_{70} and the two most influential parameters, building coverage and n, revealed a few interesting features; influence of building coverage on t^*_{70} is reduced at low n values while variation in t^*_{70} decreased at low building coverages, suggesting a decreasing influence of other urban characteristics.

Results obtained from the urban runoff study provide valuable insight on the design of flood-resilient urban environments. Reduction of t^*_{70} implies efficient conveyance of surface runoff to storage areas and can be achieved by careful design of the parameters considered in our study. Suggested measures include reduction of n by 'smoothening' existing paved surfaces, imposing upper limits on building coverage and design of advantageous street networks, aligned along slope directions.

Surface runoff in urban environments is highly complex and is affected by multiple parameters. This project successfully identified and quantified the influence of a number of urban parameters on rainfall-runoff processes, providing valuable knowledge on the design of flood-resilient urban areas in the future.

Table of Contents

1 Introduction

1.1 Background

Urban flooding has become a pressing issue due to unsustainable urban expansion and an increase in heavy localised rainfalls due to climate change. In the UK, it is predicted that both intensity and frequency of storm events during winter months will increase (Jenkins *et al.*, 2008). Urbanisation is also expected to increase at an alarming rate, as the proportion of people living in urban areas will increase to 66% of global population by 2050 (United Nations, 2014). Increasing urbanisation implies an increase in impervious, paved surfaces. This has the effect of reducing the amount of infiltrated rainfall water, as more water is accumulated over the ground, increasing surface runoff. This, coupled with an ineffective drainage infrastructure, increase the risk of urban flooding during heavy localised rainfalls.

Historically, flood risk studies in the UK have mainly been focused on fluvial and coastal flooding (Douglas *et al.* 2010). It is estimated, however, that 40% of the damage costs arising from flooding events are attributed to surface-water flooding (Environment Agency, 2007), which places at risk 2.8 million properties in England alone (EA, 2009). While the UK legislation has recognised the costs related to surface-water flooding and has called for mitigation measures, progress remains at a research level. This is mainly focused on the improvement of drainage infrastructure, with little focus on the influence urban patterns have on rainfall-runoff processes and urban planning.

The increasing availability of high resolution topographic data and advancements in computational capabilities pave the way for more detailed studies of rainfall-runoff processes, which will provide valuable insight for sustainable urban planning and design of drainage infrastructure.

1.2 Previous research

Study of rainfall-runoff processes has been object of research for the past few decades. Before the development of computing techniques, studies relied largely on simplified models and empirical relationships derived from historical hydrological data. These models were extensively validated against idealised, small-scale experimental setups.

Despite generally showing good agreement with the experimental results in idealised catchments, these models were unable to capture rapid flow changes and therefore unable to predict flow behaviour in complex topographies.

Significant advances in computational capabilities allowed the development of more complex physical methods and solution of sophisticated equations with the use of numerical schemes. For the modelling of rainfall-runoff processes there are two approaches: a classical shallow water model and an anisotropic porous model. The classical model delivers more accurate results at the expense of longer computational times whilst the latter is more computationally efficient, with the ability of maintaining a reasonable accuracy through the introduction of an appropriate porosity term (Liang *et al.*, 2016).

Shallow water equations (SWEs) describe the evolution of an incompressible fluid in response to gravity, bed friction and inertia. They have been extensively used in simulating large-scale overland runoff and have shown to be particularly suitable for predicting rainfall-runoff flow in urban environments (Cea *et al.*, 2009). With the increasing availability of high resolution topographic data, 2D SWEs have become the most popular model to model inundation flow in urban areas. Solving SWEs is, however, computationally demanding. This limits the computational resolution when conducting simulations over large areas.

Research on rainfall-runoff processes using computational methods has been mainly focused on simulating flooding scenarios over specific high-risk locations. Mitigation measures are then suggested based on the severity of the simulation results. While studies on surface flooding consider multiple factors, they disregard the influence of urban characteristics. During the last few years, there have been attempts at tackling the surface flooding problem through parametric approaches. Parametric studies enable the examination of the combined effect of various factors on rainfall-runoff processes in urban environments. Initially, this was limited to research on idealised catchments. Huang *et al.* (2014) studied the impact of building coverage on the water depths for a rectangular flume with a regular array of buildings acting as obstacles. The evolution of water depths and blockage effects were then described as a function of one parameter, building coverage.

Similarly, Liew (2017) and Lam (2016) conducted rainfall simulations on three different idealised "building" arrangements: regular, staggered and random. These are shown in Figure 1, with buildings shown in red:

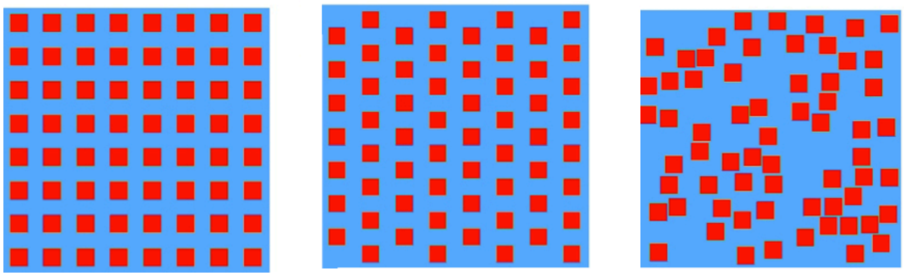

Figure 1. Regular (left), staggered (middle) and random (right) arrangements

The influence building coverage the time to reach 70% of saturated flow, was analysed by varying building coverage for each arrangement. Overall, there was a positive correlation between time and building coverage for all three arrangements. Disparities amongst these relationships in all three arrangements were mainly due to blockage effects from the narrow gaps between buildings. While best-fit curves explaining the relationships for all of the arrangements were established, it is unclear how these results relate to realistic urban configurations, where the degree of randomness varies considerably.

Bruwier *et al.* (2017) are among the first to perform a parametric study on realistic urban configurations (example shown in Figure 2). Using an anisotropic porous model, they investigated the influence of several urban pattern characteristics on inundation depths along the upstream boundaries. A steady inflow of water was prescribed at the inlet of the catchment (shown in red), representing a flood front. The sensitivity of the inundation depths to 11 urban parameters was then quantified.

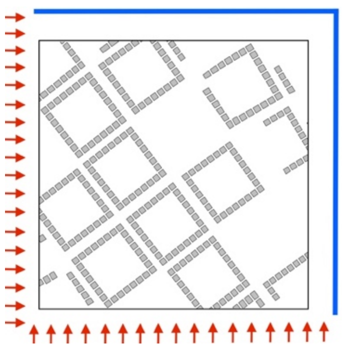

Figure 2. Example of boundary conditions used in Bruwier et al. (2017)

1.3 Objectives

Real urban environments are highly complex and it is likely that there are numerous parameters that influence the rainfall-runoff processes, e.g. urban characteristics such as road width, orientation or building coverage.

Therefore, the main objective of this project was to perform a parametric study on rainfall-runoff processes in urban environments, in order to gain a better understanding of the impact urban pattern geometry has on the flow of surface runoff. Conducting a high number of computational simulations will unveil the dominating urban parameters that influence flooding in urban systems, while performing a sensitivity analysis on the simulation results will quantify the influence of each parameter. The outcomes of this project will provide useful guidelines for the design of future flood-resilient urban environments and the improvement of existing drainage systems in cities.

2 Hydrodynamical model

2.1 Shallow water equations

The two-dimensional (2D) shallow water equations (SWEs) are a set of partial differential equations, derived based on the principle of conservation of mass and momentum in two horizontal directions. They describe the evolution of an incompressible fluid in response to gravity, bed friction and inertia. The SWEs have been extensively used in predicting large-scale inland flow processes. With the increasing availability of high resolution topographic data, 2D SWEs have become the most common model to model inundation flow in urban areas.

The 2D SWEs used in this study make use of a depth-averaged dynamic wave approximation, as was shown by Cea *et al.* (2009) to be particularly suitable for predicting rainfall-runoff in urban environments. Additional assumptions include negligible Coriolis, wind and viscous forces and assumption of a small water depth H, so that vertical momentum exchange can be ignored. As defined in Liang *et al.* (2006), the general form of the 2D SWEs ca be described using the three equations below, where Equation 1 implies mass conservation and Equations 2, 3 imply conservation of momentum in x and y directions, respectively:

$$\frac{\partial \eta}{\partial t} + \frac{\partial q_x}{\partial x} + \frac{\partial q_y}{\partial y} = 0 \tag{1}$$

$$\frac{\partial q_x}{\partial t} + \frac{\partial \left(\frac{\beta q_x^{\ 2}}{H} \right)}{\partial x} + \frac{\partial \left(\frac{\beta q_x q_y}{H} \right)}{\partial y} = -gH \frac{\partial \eta}{\partial x} - \frac{g q_x \sqrt{q_x^{\ 2} + q_y^{\ 2}}}{H^2 C^2} \tag{2}$$

$$\frac{\partial q_y}{\partial t} + \frac{\partial \left(\frac{\beta q_x q_y}{H} \right)}{\partial x} + \frac{\partial \left(\frac{\beta q_y^{\ 2}}{H} \right)}{\partial y} = -gH \frac{\partial \eta}{\partial y} - \frac{g q_y \sqrt{q_x^{\ 2} + q_y^{\ 2}}}{H^2 C^2} \tag{3}$$

In the above equations, η is the water surface elevation above datum; H is the total water column depth equal to $h+\eta$, with h being the water depth below datum; q_x and q_y are the unit width volumetric flow rate in x and y directions, respectively; C is Chézy coefficient, describing surface roughness; β is a correction factor for the nonuniform velocity profile (1.0 for a uniform velocity distribution and 1.016 for a seventh power law velocity distribution); and g=9.81 m/s^2 is gravitational acceleration.

2.2 Numerical scheme

For the numerical solution of the partial differential equations (SWEs), a Total Variation Diminishing (TVD) MacCormack finite difference numerical scheme is applied. This scheme is capable of solving the non-linear SWEs at a high efficiency and has been extensively validated against published experimental and analytical results. Detailed implementation of the numerical scheme and details of the numerous validation tests can be found in Liang *et al.* (2006).

The scheme is not unconditionally stable and stability can be ensured by restricting the maximum time step according to the Courant-Friedrich-Lewy (CFL) condition:

$$\Delta t \leq \frac{\Delta x}{\max\left(\frac{\sqrt{q_x{}^2 + q_y{}^2}}{H} + \sqrt{gH}\right)} \tag{4}$$

where Δt is the time step; Δx is the grid size; and other terms as defined above in Section 2.1. Both time step Δt and grid size Δx are specified as inputs, while H, q_x and q_y are outputs of the numerical simulation, i.e. not available prior to the simulation. Therefore, Δt was often estimated based on past experience, depending on Δx and the estimated flow field of the domain.

2.3 Method of representing buildings and obstacles

In order to represent buildings or obstacles, the building-hole (BH) method was used, where the grid cells representing buildings are excluded from the computation. The elevations of these grid cells are then increased in order to prevent any flow of water into these 'holes'. Where necessary, the rainfall intensity over the whole domain was increased to compensate for the 'loss' of rainfall falling over these 'holes'. A different approach is the building-block (BB) method, where shapes of the buildings are treated as part of the topography and rainfall is applied over the whole domain. Although BB is a more physically realistic approach, it requires local mesh refinement around the buildings and is therefore less efficient numerically (Cea *et al.*, 2009).

Small-scale microtopography due to obstacles in urban environments e.g. cars, trees, debris is not considered separately, but instead a uniform roughness coefficient over the whole domain is chosen to account for the various sources of flow resistance. In the first validation example of this study, the value of roughness $n = 0.04\ m^{-1/3}s$ was used, comparable to the values suggested by Bazin (2013) and Mignot *et al.* (2006). In the subsequent sections of this report, roughness was varied to determine its influence on the hydrological behaviour of the catchment.

2.4 Pre-processing methods

Each computational simulation requires as input a text data file of a standardised format. This specifies four main components: simulation parameters, boundary conditions, domain description and initial conditions.

Simulation parameters include specification of numerical parameters such as time step Δt, grid size Δx and momentum correction factor β as well as physical parameters and rainfall intensity. In order to ensure flow will be contained within the domain and will only leave domain where required, it is essential to impose correct boundary conditions. These include specifying the unit width volumetric rate (q_x, q_y) along the cells in each boundary to be zero or prescribed according to a rating curve, depending on the problem analysed. Domain is specified as described in Section 2.3, where grids consisting of buildings/obstacles are excluded from the computational domain. Finally, initial conditions specify the initial topography of the domain by specifying the elevation at each grid point in the domain. The BH method is then applied, where elevation of buildings/obstacles is increased to prevent flow of water into the 'holes'.

The domains considered in this project were mainly realistic urban layouts, consisting of irregular arrays of buildings. As will be shown later in this report, they were obtained in a shapefile format, comprising of polygons, polylines and points defining each grid point in the domain. In order to enable their use for our study and make them compatible with the standardised format mentioned above, the methodology shown in Figure 4 was followed:

Firstly, the shapefiles were converted into raster format, comprising of pixels. This was done through a workflow generated using FME, a data processing software, shown in Figure 3 for three building layouts. This enabled batch conversion of the shapefiles and the ability to specify the desired resolution and attributes of the resulting image.

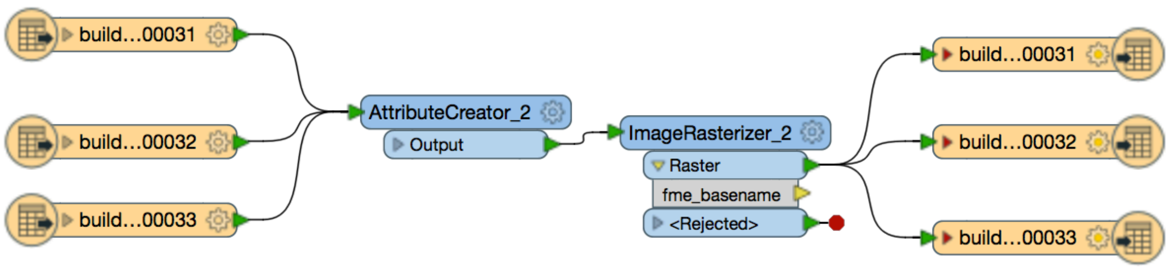

Figure 3. Example of FME workflow for three urban layouts

Image processing using a code written on Matlab was then used to generate a binary image of 1s and 0s to describe the domain occupation (1s representing the flow domain and 0s representing the buildings). Subsequently, the domain was modified to accommodate the desired boundary conditions and finally, assembled into an input file through a Matlab script. This involved specifying initial conditions for each one of the grid points in the domain The domains used in this study were of high resolutions, with the number of grid points in the order of millions, requiring in this way significant computational effort. This was avoided through the use of a vectorised approach throughout the assembly of the Matlab code, reducing computational times significantly. Overall, the methodology followed for the preparation of an input file for each configuration is visualised in the flow chart below:

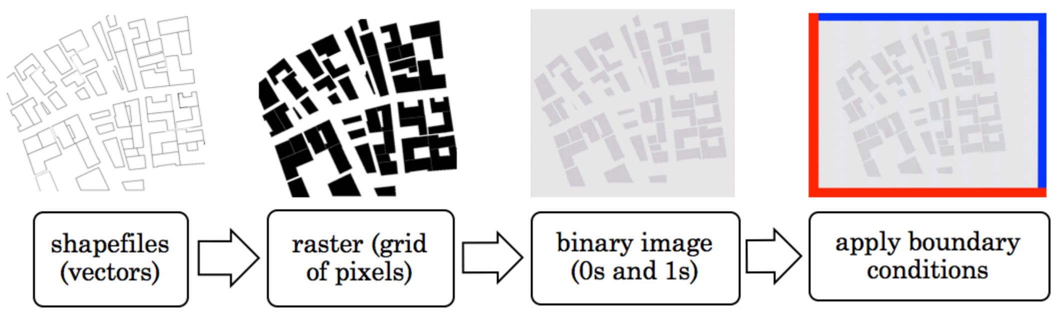

Figure 4. Methodology for input file preparation

2.5 Post-processing methods

The output of the numerical simulation comprises of a file containing flow rates q_x and q_y and water elevation η at each grid point for every time step. This was standardised to a format readable by Tecplot, a powerful CFD visualisation and analysis software. The numerical file was then loaded by Tecplot, which visualised the evolution of the flow field in the domain. Analysis of the results was possible through the built-in functions of the software. Integration of the flow rate q_x at each grid point for every time step along the downstream boundary yielded the hydrograph of the catchment. This was then used to determine the time to reach 70% of the steady flow rate, which was used in this study to characterise the rainfall-runoff response.

When dealing with a large number of simulations, automation of the process was crucial. This was done through a macro script on Tecplot (Appendix A) while a Matlab script was written to determine the time to reach 70% of the steady flow rate for each hydrograph.

3 Urban layout generation and model validation

3.1 Realistic urban layout generation

As explained in Section 1.3, one of the first objectives of this study is to conduct simulations on realistic urban layouts. Therefore, the first stage of the study is focused in the generation of realistic urban layouts.

Initially, realistic urban forms were generated using available literature and software. For the generation of virtual urban systems, it is widely suggested the use of procedural modelling, which automatically generates urban networks given a set of rules (Prusinkiewicz, 1990). CityEngine, a procedural modelling software, was used to generate parametrised urban configurations, one example shown in Figure 5a. However, only three parameters (road width, building coverage, building shape) can be used and the configuration does not resemble real-life urban configurations.

OpenStreetMap, an open source collaborative project, enables the generation of real-life urban forms, as shown in Figure 5b. Urban forms are generated through crowdsourcing, by tracing building and street boundaries from available satellite maps of urban environments. This is particularly useful when predicting the rainfall-runoff behaviour of specific real-life urban environments. However, these environments are highly complex and virtually impossible to parametrise, thus not particularly useful for a parametrised study.

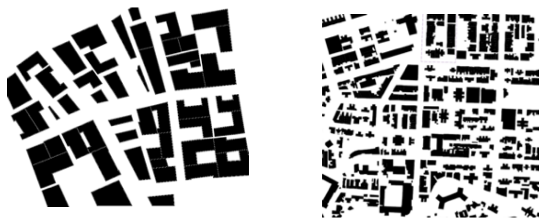

Figure 5a, b. Generated urban forms

A recent paper, *"Influence of urban patterns on floods"* (Bruwier *et al.*, 2017) presented at the 37th International Association for Hydro-Environment Engineering and Research (IAHR) World Congress, examined hydraulic computations on 2,290 urban configurations using an anisotropic porosity model. Urban configurations were generated by means of a self-developed urban generator tool, based on the procedural modelling technique explained above. This was followed by a parametrised study using 11 urban parameters controlling the building geometries and locations, shown in Table 1. Each of the parameters was randomly selected from a range of variation, representative of real-world information of built environments.

Table 1. Range of parameters used in the urban generator

Input parameters and building coverage for the urban generator engine.

ID	Parameter	Minimum value (P_{min})	Maximum value (P_{max})
P1	Averagestreet length	40 m	400 m
P2	Street orientation	0°	180°
P3	Street curvature	0 rad.	0.42 rad.
P4	Major street width	16 m	33 m
P5	Minor street width	8 m	16 m
P6	Park coverage	5%	40%
P7	Maximum parcel area	300 m^2	1,100 m^2
P8	Building front setback	0 m	5 m
P9	Building rear setback	0 m	5 m
P10	Building side setback	0 m	5 m
BC	Building coverage	0%	42.8%

Following the generation of urban configurations, Bruwier *et al.* (2017) applied steady inflow of water across each configuration and recorded the resulting steady state inundation depths and velocities recorded. The influence of each parameter on the inundation depths along the upstream boundaries was then quantified.

Although the study considers steady inflow into the domain and not rainfall events over the domain, the urban configurations generated by the tool can be suitable for our rainfall-runoff analysis. Directly contacting the author of the paper and signing a written agreement enabled direct access to all of the 2,290 urban configurations, developed at Purdue University by the team of Prof. Daniel G. Aliaga. The urban layouts were obtained in a shapefile format and were subsequently converted to the format compatible with the model used in this study, as was shown in Section 2.4 of this report. These configurations served as a starting point for the rainfall-runoff parametric study, as will be analysed later in this report.

Figure 6. Examples of urban tool configurations

3.2 Model validation

In order to examine the accuracy and stability of our classical model with the above configurations, a number of simulations were performed under the same boundary conditions as Bruwier *et al.* (2017). This involved application of a steady flow across the domain and comparison of the resulting inundation depths. Validation of steady flow results was conducted on a number of configurations for which results were available.

In the subsequent section, simulations were conducted on a V-shaped watershed under different slope and rainfall combinations. The resulting outflow hydrographs from the slopes of the watershed were validated against empirical kinematic models obtained by Henderson & Wooding (1964) as well as Overton & Brakensiek (1970).

3.2.1 Bruwier *et al.* (2017)

Bruwier *et al.* (2017) used an anisotropic porous model to investigate the influence of several urban pattern characteristics on inundation depths along the upstream boundaries of the catchment. The boundary conditions applied were: uniform zero slope, a steady inflow of 200 m^3/s prescribed along the upstream boundary (shown in red in Figure 7) and a uniform roughness n = 0.04 $m^{-1/3}s$ across the domain. The specific discharge q_j across the downstream boundary (shown in blue in Figure 7) was specified according to the following rating curve function:

$$q_j = C_1 \Delta x \sqrt{2g(H_j - C_2)^3} \tag{5}$$

where sub-index j indicates the value at cell j, grid spacing is Δx; constants C_1 = 0.5 and C_2 = 0.3; and H_j is the computed water depth in cell j. Finally, an outer strip of thickness = 3% of the domain of size 1km x 1km, was added for the convenience of implementing the outflow boundary condition, as shown below:

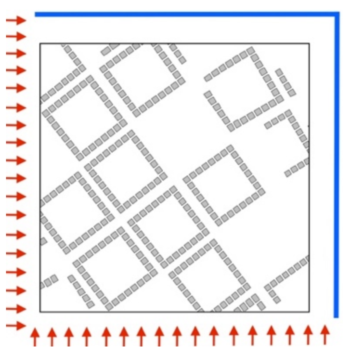

Figure 7. Prescribed boundary conditions

3.2.1.1 Simulation instabilities

Initially, the simulations were prone to instabilities, causing their termination. However, careful investigation of the instability through its visualisation using data visualisation software Tecplot revealed the cause, shown in Figure 8, with the water depth *H* in metres and buildings shown in red. As water approaches the upper and right downstream boundary, it is forced through a narrow passage of 1s, representing small gaps between buildings. This, coupled with the applied boundary conditions in the downstream boundary, generated unusually high water depths and eventually terminated the simulation. Using a higher resolution of the input binary image gave a better representation of the gaps and resolved the issue, though at much longer computational times.

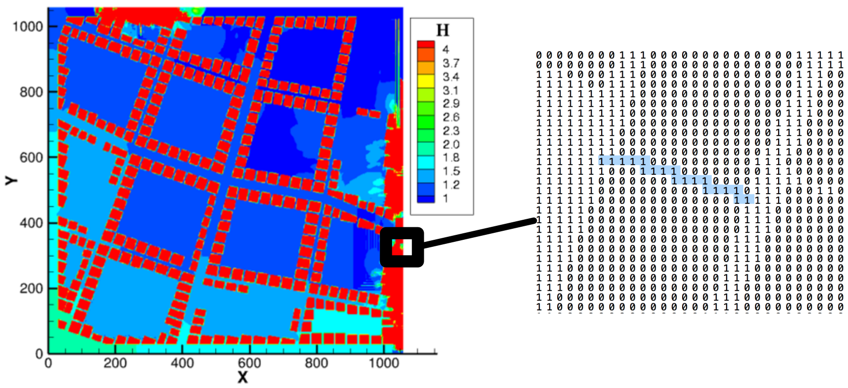

Figure 8. Unstable flow visualisation and the binary input file (right)

3.2.1.2 Stable results

Stable results were obtained using an additional thin layer of the flow domain and a higher resolution (1m x 1m cells) under the boundary conditions discussed above. This enlarged the narrow gaps between buildings and allowed the flow of water into these narrow passages. Visualisation of the resulting steady state depths (contours) and

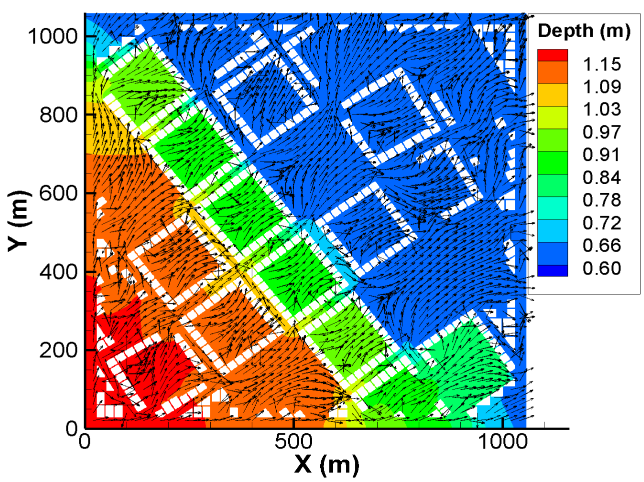

Figure 9a. Flow visualisation configuration A

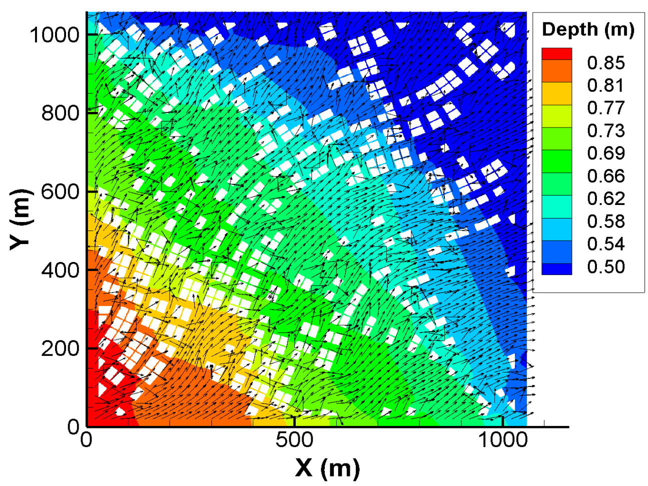

Figure 9b. Flow visualisation configuration B

velocities (vector arrows) is shown in Figures 9a, b, c for three configurations A, B and C, with buildings shown in white:

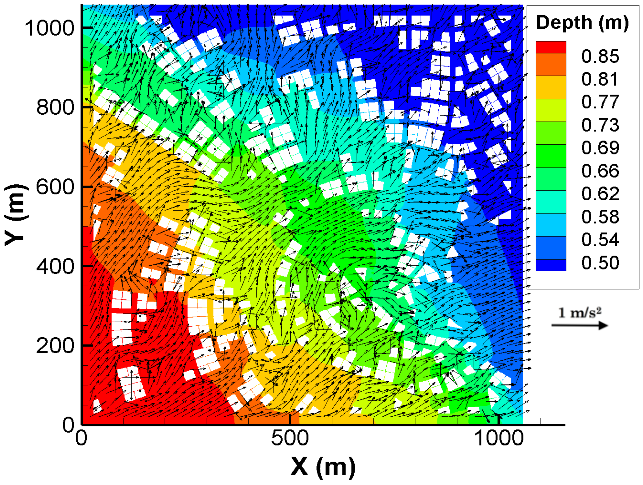

Figure 9c: Flow visualisation configuration C

As seen in the figures above a more advantageous street and building orientation can reduce innundation depths significantly. For example, flow of water across the lower left upstream boundary in configuration A is obstructed by the block of buildings, resulting in considerably greater water depths reaching more than 1.15 metres. This is not the case for B and C where buildings are distributed across the domain, allowing easy flow of flood water towards the downstream boundaries and lower water depths as a result.

In order to compare simulation results for different configurations, Bruwier *et al.* (2017) used h_{90}, the 90th percentile of water depths in each cell of the upstream boundaries. A similar approach was followed in this study and water depths along the upstream boundary (starting from top left to bottom right of the domain) were initially plotted, shown in Figure 10:

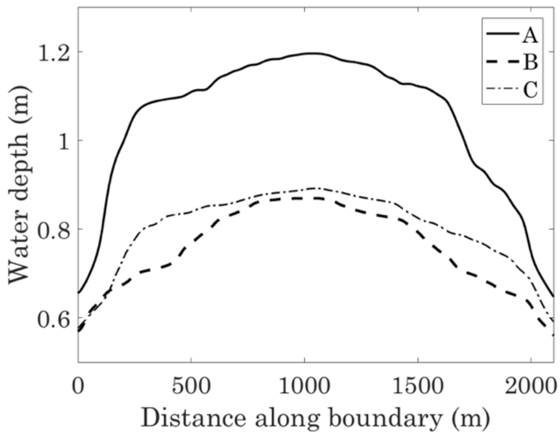

Figure 10. Water depth along upstream boundary

Subsequently, h_{90} was calculated for all three curves and compared with the porous model results obtained in Bruwier *et al.* (2017), as shown below in Table 2:

Table 2. Comparison of h_{90} values for A, B, C

	h_{90} (90th percentile of upstream depths in metres)	
Configuration	*Classical model*	*Porous model*
A	1.18	0.79
B	0.87	0.74
C	0.88	0.75

The results agree reasonably closely for configurations B and C, with higher values in the classical model. One reason for this is the difference between the porous and classical model. The former uses a lower resolution (2m x 2m cells) and introduces porosity terms to maintain reasonable accuracy. This has a slight 'shrinkage effect' on buildings, allowing more possible paths for water flow. In the high resolution classical model, the topography of the urban layout is perserved, resulting in greater depths along upstream boundaries. As expected, the difference between the models is more prominent in the more dense case A, where upstream water depth is highly sensitive to the presence of the block of buildings near the upstream boundary. Overall, it can be concluded that the results generally agree between the models and the capability of the classical model in simulating prescribed water flow is largely confirmed.

3.2.2 Kinematic surface runoff model

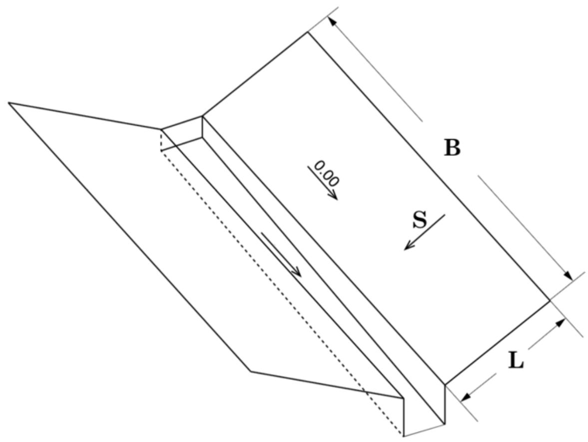

Figure 11. Geometry of the V-shaped channel

Henderson & Wooding (1964) developed a kinematic model to predict the build-up and decay of laminar or turbulent flow over an impermeable sloping plane. This allowed the development of an approach to determine the behaviour of a V-shaped watershed (Figure 11) due to uniform constant rainfall. Results from the kinematic model generally showed good agreement with observed runoff hydrographs from natural V-shaped watersheds.

The hydrological response of the entire watershed can be considered as the combined response of overland flow over the sloping planes and the subsequent flow over the 'collection' channel. Rainfall on the sloping planes will induce runoff flow, which will result in two identical outflow hydrographs at the bottom boundary of the two identical planes. Outflow from the edge of the planes serves as inflow to the channel, developing a different hydrograph at its outlet, at the same steady outflow rate but at with a 'delayed' time of concentration.

In this study only the response of one sloping plane under a uniform, constant rainfall of finite duration was considered, shown in Figure 12:

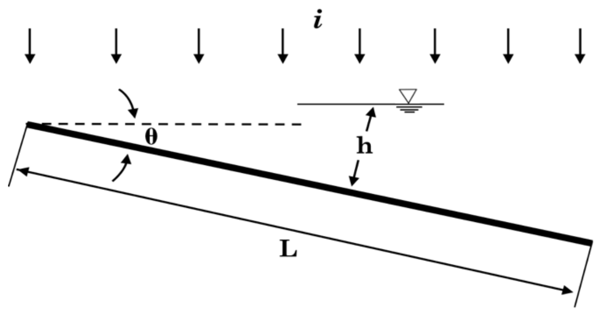

Figure 12. Rainfall flow over a sloping plane

The assumptions made in the kinematic model were:

1. Depth of water is sufficiently small so the slope of the water surface relative to the slope of the plane can be neglected.
2. Plane surface is impermeable.

3. Impact of raindrops on the surface and acceleration terms in the flow equation are neglected.
4. Rainfall intensity i is constant.

From the assumptions above, Henderson & Wooding (1964) showed that the specific flow rate can be expressed as a function of depth h:

$$q = \alpha h^m \tag{6}$$

where a is a function of slope S, depending on the type of flow assumed: laminar, turbulent, or flow in a porous medium; m is a constant, also dependent on the type of flow. In this study, m was chosen to be 1.5, corresponding to turbulent flow (Henderson & Wooding, 1964).

3.2.2.1 Derivation of mathematical model

In order to obtain the mathematical description of the different portions of the plane hydrograph, work done by Overton & Brakensiek (1970) was consulted, who developed a similar kinematic surface runoff model. It was shown that the hydrograph of the watershed reaches steady state at time t_{eq}:

$$t_{eq} = \frac{0.928}{i^{0.4}}\left(\frac{nL}{\sqrt{S}}\right)^{0.6} \tag{7}$$

where n is the Manning roughness coefficient in $m^{-1/3}s$; L is the length of the plane as defined above in feet; i is the rainfall intensity in inches/hour; and S is the slope of the plane. The outflow Q in m^3/s for the rising curve of the hydrograph and the equilibrium flow rate from rainfall of duration t_i will then be:

$$0 \le t \le t_{eq} \qquad Q = i \cdot A\left(\frac{t}{t_{eq}}\right)^m \tag{8}$$

$$t_{eq} \le t \le t_i \qquad Q = i \cdot A \tag{9}$$

Henderson & Wooding (1964) used the method of characteristics to show that the depth of water h at the bottom of the plane evolves according to the equation:

$$L = \alpha h^{m-1}\left(\frac{h}{i} + mt_c\right) \tag{10}$$

where t_c here is the time after the cessation of rainfall, also equal to overall time t minus t_i, the duration of rainfall. Combining Equations 7-10, the outflow Q at the bottom of the plane was obtained, shown below in implicit form:

$$mt \cdot \left(\frac{i \cdot A}{Q}\right)^{1/m} = t_{eq} \cdot \left(\frac{i \cdot A}{Q} - 1\right) \tag{11}$$

3.2.2.2 Comparison of results

Using Equations 8, 9 for the rising and equilibrium portion of the hydrograph and Equation 11 for the decay portion, the analytical hydrographs can be obtained and compared to the simulation results. For the simulation, an 800m x 1000m plane of uniform slope S and roughness n was considered and simulations were conducted at a 10 metre resolution. Uniform constant rainfall was applied for 2500 seconds over eight different combinations of slope S, intensity i and roughness n.

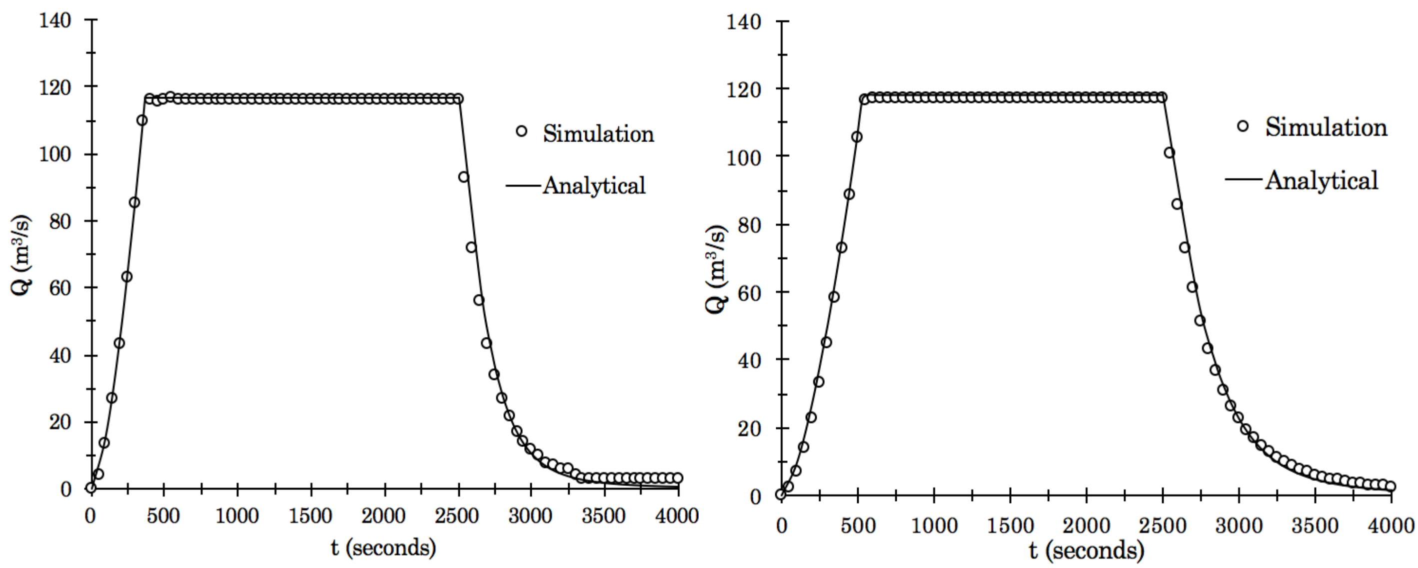

(a) n = 0.015 sm$^{-1/3}$, S = 0.05 (b) n = 0.020 sm$^{-1/3}$, S = 0.025

Figure 13. Hydrographs for constant rainfall i = 540 mm/h

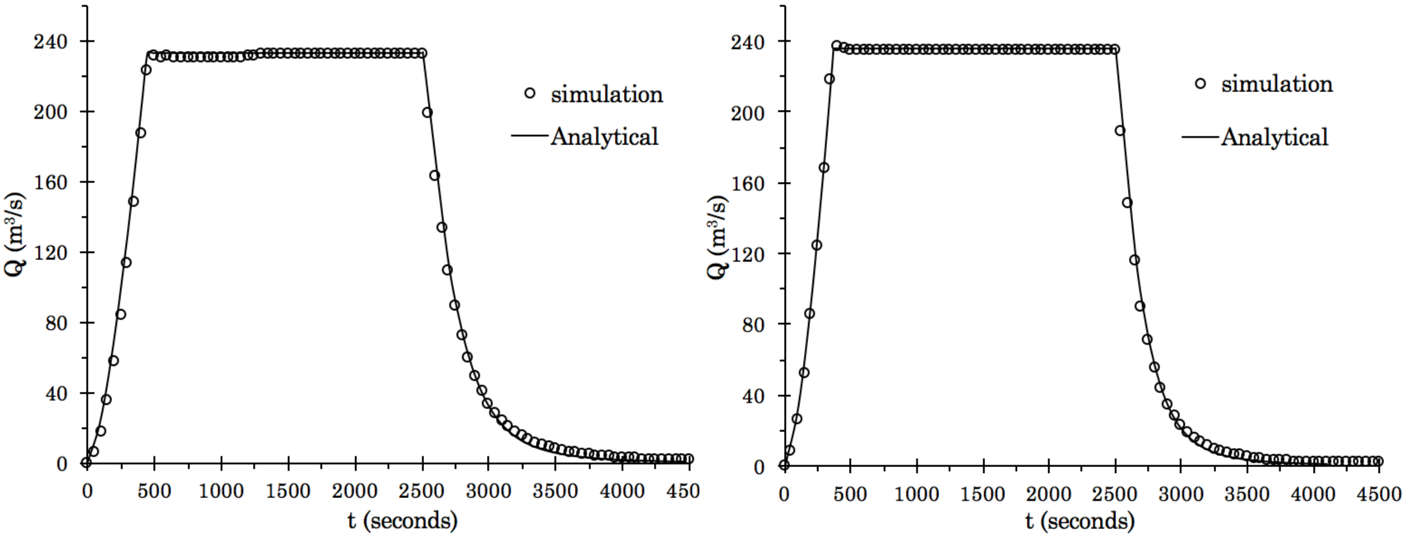

(a) n = 0.015 sm$^{-1/3}$, S = 0.01

(b) n = 0.020 sm$^{-1/3}$, S = 0.035

Figure 14. Hydrographs for constant rainfall i = 1080 mm/h

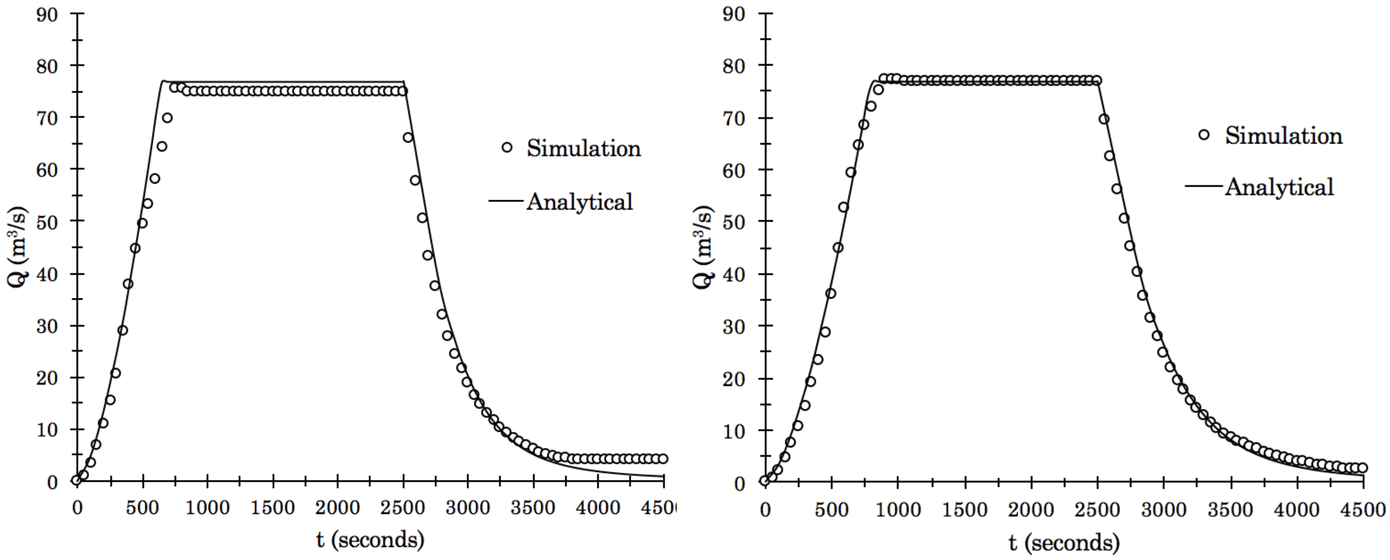

(a) n = 0.025 sm$^{-1/3}$, S = 0.035

(b) n = 0.030 sm$^{-1/3}$, S = 0.025

Figure 15. Hydrographs for constant rainfall i = 360 mm/h

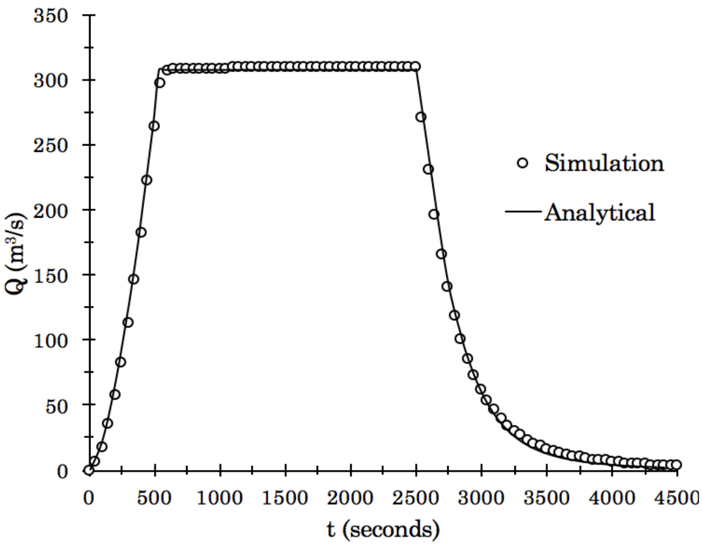

(a) n = 0.025 sm$^{-1/3}$, S = 0.01

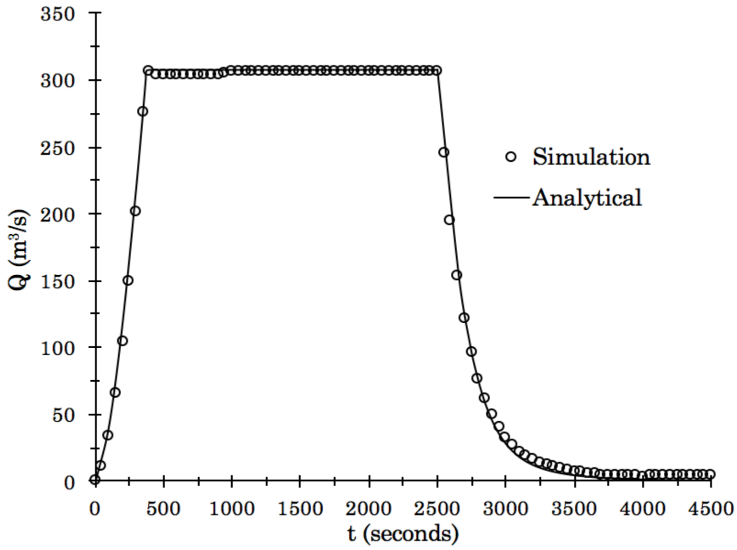

(b) n = 0.030 sm$^{-1/3}$, S = 0.05

Figure 16. Hydrographs for constant rainfall i = 1440 mm/h

As seen from Figures 13 - 16, the shape of all simulated hydrographs matched the analytical hydrographs. Good agreement was observed in all of the portions of the hydrographs: the rising limb, time to reach the peak flow rate, value of the peak flow rate and the falling limb. Slight differences were seen in the falling limb, at very low flow rates; the numerical simulation results level off to a constant value. This is more noticeable in the hydrograph of low rainfall intensity, as seen in Figures 13a, 15a. However, this only occurs at low flow rates, likely to be caused from numerical approximation at very low water depths.

Overall, it can be concluded that the numerical results closely agree with the analytical solutions. This confirms the capability of the model in simulating overland flow and predicting the outflow hydrograph of an impermeable sloping plane under uniform, constant rainfall of a finite duration.

3.3 Re-examination of *S*-curve normalisation theory

3.3.1 Hydrograph theory

If continuous rainfall of intensity i falls uniformly over an impervious area A, the discharge from the basin will, after a time, reach equilibrium. This is due to the volumetric outflow rate equating the volumetric rate of rainwater introduced to the catchment. The resulting steady outflow rate Q will then be:

$$Q = i\,A \tag{12}$$

The time to reach the equilibrium is known as *'the time of concentration',* roughly equal to the time taken for the raindrop falling on the furthest part of the catchment to reach the outlet. The time of concentration t_c can be illustrated in the cumulative hydrograph below, also known as the S-curve:

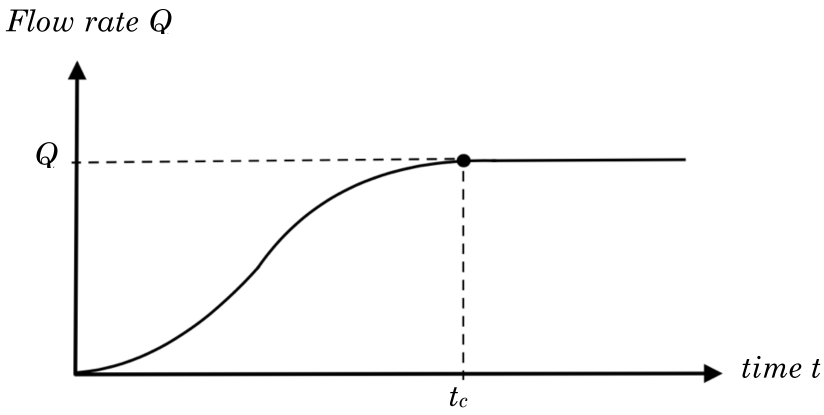

Figure 17. S-curve for a catchment under continuous rainfall

3.3.2 Dimensional analysis

The hydrograph resulting from short-lived rainfall over an impervious catchment contains mixed information about the rainfall intensity and duration as well as the landscape properties of the catchment. In order to avoid time dependency on the problem, it is convenient to consider unceasing uniform rainfall, resulting in a S-curve as shown above. The hydrological response of the catchment will then be dependent on the following independent variables: rainfall intensity, size and slope of the catchment, ground roughness and geometry of the obstacles in the catchment. By conducting numerous simulations on the same catchment with constant ground roughness n, we can compare the hydrological response as a function of rainfall intensity i (m/s), size of the catchment (m), slope S of the catchment and finally gravitational acceleration g (m/s^2).

The catchment chosen for the dimensional analysis is a square building arrangement, shown in Figure 18. A thin 'layer' surrounding the buildings was added, in order to prevent any 'blockage' of the water path at the boundaries. Uniform unceasing rainfall of intensity i was applied across the square domain of uniform roughness n = 0.04 m$^{-1/3}$s and slope S in the direction shown in Figure 18. The boundary conditions consisted of preventing flow of water across the upper and lower boundaries and critical flow condition across the right 'outlet' boundary.

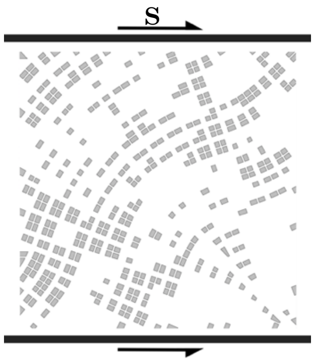

Figure 18. Urban layout considered and slope direction

A number of simulations with different combinations of the domain slope S and rainfall intensity i were conducted on the above configuration. The resulting hydrographs at the right boundary of the domain were recorded and shown below in Figure 19.

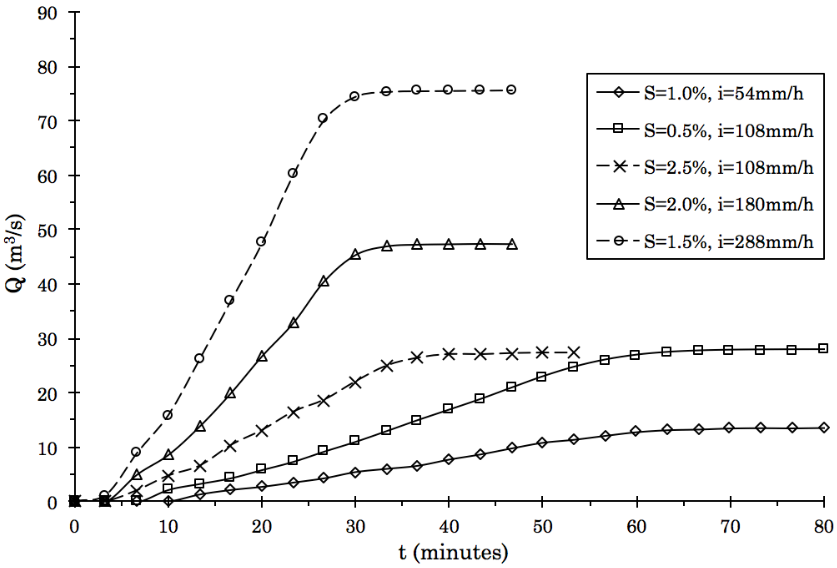

Figure 19. Hydrographs at right downstream boundary

As expected, there are significant differences between the time of concentration and steady outflow rate of the different combinations. These arise from the different combinations of rainfall intensity i and slope S. In order to enable the development of an approach that compares hydrological response based on the characteristics of the built environment, independent of the above parameters, we must follow a dimensionless hydrograph approach. The dimensionless hydrographs for the catchment in Figure 18 under different combinations of slope S and rainfall intensity i are then expected to collapse to a single curve.

Following a similar approach to Liang *et al.* (2015), two possible dimensionless variables of time and the same dimensionless flow rate were considered for this analysis. The dimensionless flow rate chosen was simply the ratio between the outflow rate and the volumetric rate of rainwater introduced to the catchment. This ranges from 0 to a maximum of 1, corresponding to steady flow beyond the time of concentration. This is shown in Equation 13 where Q = flow rate across outlet, A = catchment area and i = rainfall intensity.

$$Q^* = \frac{Q}{A \cdot i} \tag{13}$$

Initially, the dimensionless time in Equation 14 was considered, comprising of time t, rainfall intensity i and domain area A (in this case simply the area of the square):

$$t^* = \frac{t \cdot i}{\sqrt{A}} \tag{14}$$

The second dimensionless time is shown in Equation 15, encompassing time t, domain slope S, gravitational acceleration g and domain area A:

$$t^* = \frac{t \cdot \sqrt{S \cdot g}}{A^{0.25}} \tag{15}$$

The resulting dimensionless hydrographs from first and second approaches are shown in Figures 20, 21, respectively. The shape of the S-curves using the first dimensionless time are clearly distinct and do not collapse to a single curve. This is as a result of the dependence of the dimensionless time on rainfall intensity and inability to capture the changing slope of the different combinations considered.

The more physical approach, comprising of the catchment area A as well as the gravitational component along the direction of flow along the slope $S \cdot g$, succeeds in converging the S-curves into a single curve (as seen in Figure 21). This is more noticeable in the increasing and equilibrium portions of the hydrographs. Therefore, the second dimensionless time was used for the future stages of this study.

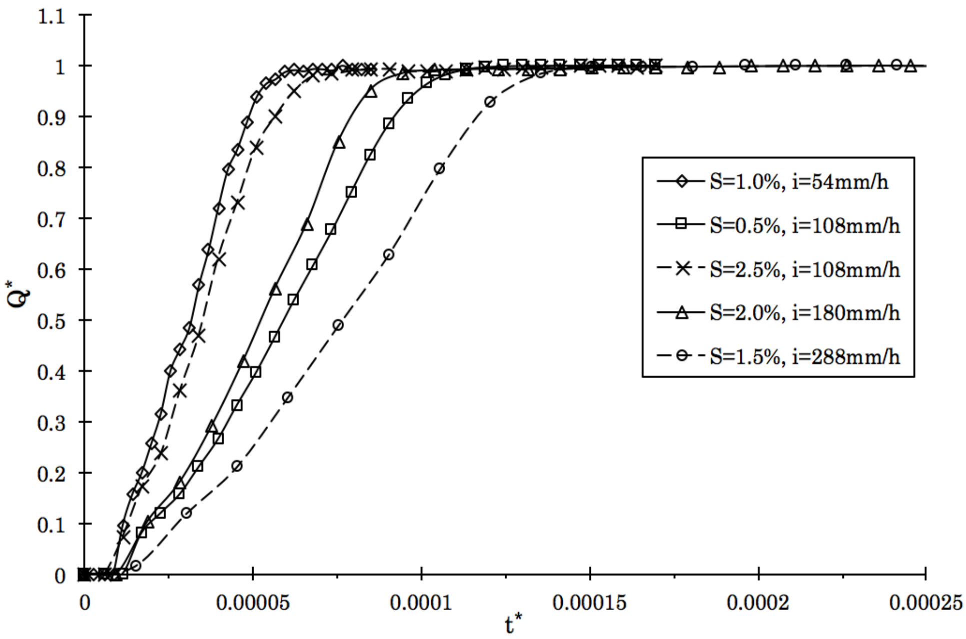

Figure 20. Dimensionless hydrograph (1st approach)

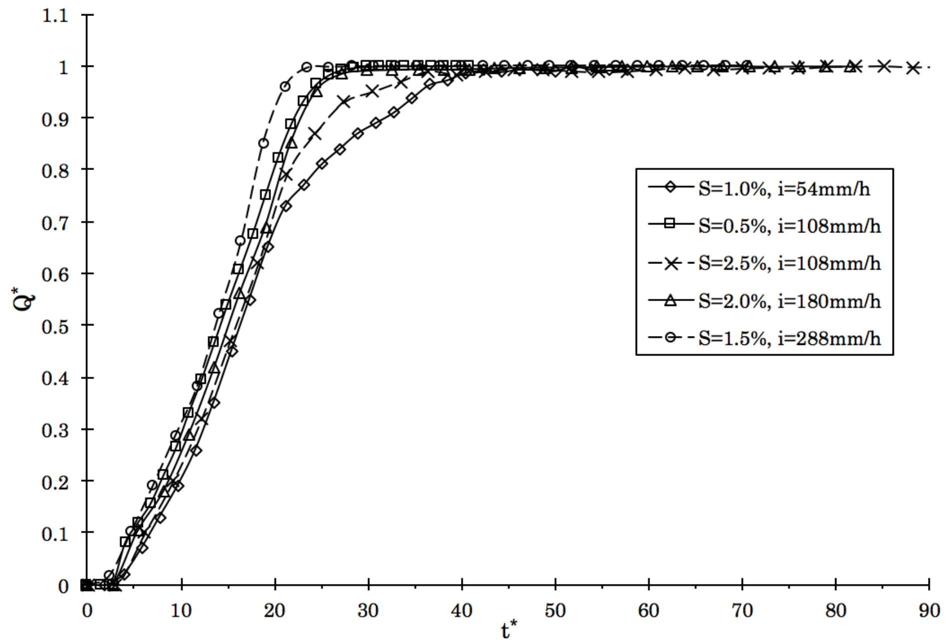

Figure 21. Dimensionless hydrograph (2nd approach)

3.3.3 Time of concentration

It was shown in Section 3.3.1 that time of concentration t_c characterises the hydrological response of the catchment, by representing the time flow rate reaches equilibrium state. While this concept is theoretically sound, it is impractical to use in real simulations. Hydrographs generally reach equilibrium state at a very low rate, also witnessed in the *S*-curves of Figures 19-21. Estimation of the full time of concentration t_c would therefore result in large errors and is not desired. It is common for researchers to use t_{25} or t_{50}, the times to reach 25% or 50% of equilibrium flow rate, respectively. However, Lam (2016) showed there is additional benefit of having a bigger variation of dimensionless time, t^*_{70}, when comparing dimensionless hydrographs of building configurations of different building areas. Therefore, time to reach 70% of the dimensionless equilibrium flow rate, t^*_{70} will be used to characterise the rainfall-runoff response in the following urban runoff study.

4 Urban runoff parametric study

Following the successful model validation and re-examination of the S-curve normalisation theory, the final stage of the project involved carrying out a sensitivity analysis to identify the influence of various urban parameters on rainfall-runoff processes. The rainfall-runoff response was characterised by the dimensionless time $t^* = t \cdot \sqrt{S \cdot g}/A^{0.25}$, following the examination of the non-dimensional rainfall-runoff relationship in Section 3.3. The sensitivity of t^*_{70} to a number of urban characteristic was then quantified using a multiple linear regression (MLR), allowing the identification of the most influential urban parameters. Use of High Performance Computing (HPC) and parallel processing enabled the simulation of 2,994 rainfall-runoff processes on 998 different urban layouts.

Initially, the simulation parameters used are presented, followed by a description of the methodology to automate the pre- and post-simulation processes. The implementation of the statistical approach and its results is then explained and the correlation between the most influential parameters and t^*_{70} examined. Finally, the implications of the results for real-life urban environments and urban planning are discussed.

4.1 Simulation parameters

It was shown in Section 3.3 that dimensionless hydrographs using t^* under different combinations of slope S and rainfall intensity i collapse to a single curve. This allows the use of any slope S and rainfall intensity i in our study, as the non-dimensional rainfall-runoff relationship is independent of these variables. However, certain combinations of slopes and rainfall intensities introduced simulation instabilities, in a similar fashion to the instabilities explained in Section 3.2.1.1. Therefore, a constant slope S = 1% in the direction shown in Figure 22 and a uniform rainfall intensity i = 108 mm/h was applied across all of the urban layouts, producing 2,994 stable results. A critical flow boundary condition was imposed across the right boundary, so the flow velocity is equal to the shallow-water wave celerity.

The domain size for all the layouts is 1km x 1km, with an additional outer strip of thickness = 30 metres. This was added for the convenience of implementing a critical outflow boundary condition, shown in red in Figure 22. To ensure a balance between accuracy and computational effort, the chosen cell size was 2m x 2m. Flow of water was also prevented out of the left, lower and upper boundaries, shown in blue.

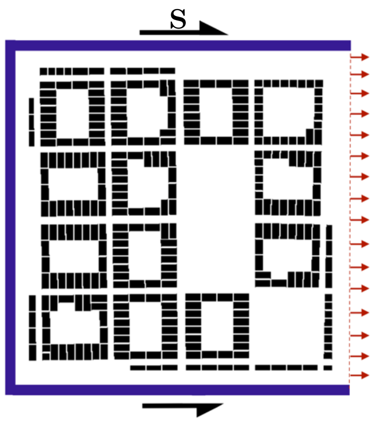

Figure 22. Applied boundary conditions and slope direction

For this study, 12 urban characteristics were used as independent variables. The first 11 variables, introduced in Section 3.1, are defined in the urban layout itself (Figure 23) and define the urban geometry. The 12th variable, Manning roughness coefficient *n* was introduced uniformly across the domain prior to the simulation as an input. In total, 998 urban layouts were computed and three values of roughness coefficient *n* were used: 0.02, 0.04 and 0.07 $m^{-1/3}s$, giving a total of 2,994 simulations. Examples of three urban layouts and their respective parameters used in the analysis are shown in Figure 23:

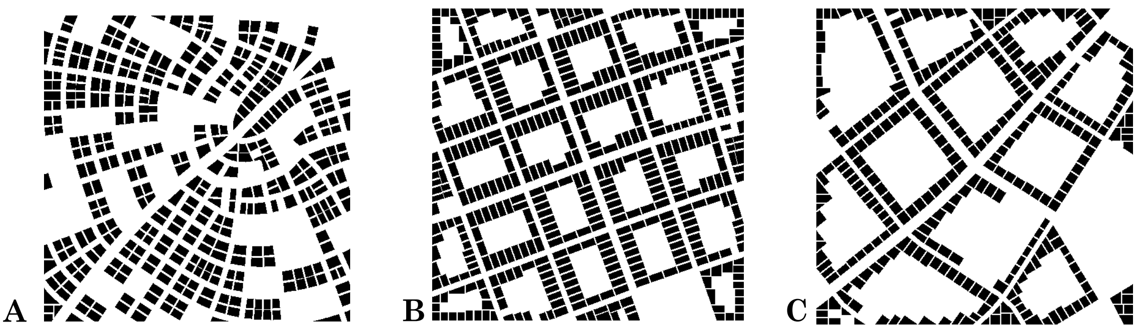

	Street length	Street orientation	Street curvature	Street width1	Street width2	Park coverage	Parcel area	Front setback	Rear setback	Side setback	Building coverage
A	75.7m	137.3°	0.31	30.4m	13.6m	26.7%	1034m²	1.3m	1.5m	3.8m	29.0%
B	212.3m	24.0°	0.051	20.7m	12.8m	10.4%	810m²	1.1m	1.9m	3.1m	34.3%
C	295.0m	155.1°	0.29	28.5m	10.3m	23.7%	898m²	1.1m	3.0m	3.0m	23.2%

Figure 23. Examples of urban parameters used in layouts A-C

4.2 Process automation

Dealing with a great number of computational simulations presents significant manpower and computational challenges. Therefore, substantial effort was dedicated to the development of an automated approach and parallel computation throughout the simulation processes. Pre- and post-simulation processes were automated by applying a vectorised coding approach and use of specialised software. Regarding simulations, HPC enabled efficient and parallel computations through the use of batch simulation techniques.

4.2.1 Pre-processing

Preparation of a single input file was done according to the methodology described in Section 2.4, the main difference here being the number of input files to be prepared. Conversion into raster format was enabled through the use of the Batch Deploy method in FME software, which allows for multiple source readers and multiple destination writers. The workflow used for the conversion is shown below in Figure 24.

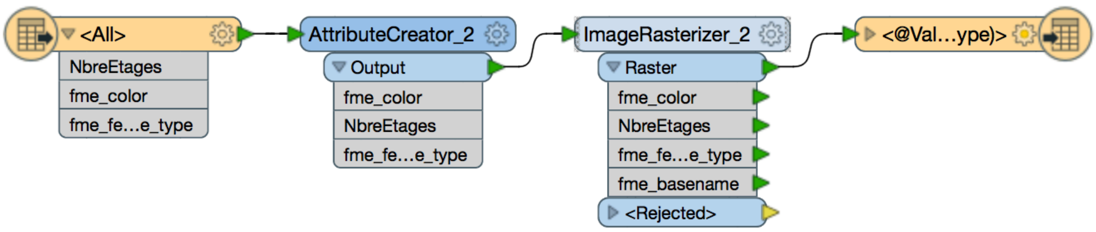

Figure 24. Example of FME workflow for batch conversion

The Matlab code developed to write the input files into a standardised format was restricted to operations involving matrices and vectors while loop-based, scalar-oriented code was always avoided. This reduced computational time considerably from the order of hours to a few seconds.

4.2.2 Batch simulation

Simulation of 2,994 rainfall-runoff processes would not have been possible without the use of HPC Darwin cluster of Cambridge University. Submission of input files for simulation was done through the preparation of a SLURM (a job scheduling system) script, comprising of the set of commands to run and resource requirements for the job submitted. The submitted jobs were then transferred to a queuing system, where concurrent simulation of a number of jobs was eventually possible, depending on the availability of computational nodes.

4.2.3 Post-processing

Tecplot, a data visualisation software, was used to visualise and process the simulation outputs, as described in Section 2.5. Again here, the main challenge was the processing time required for the generation of the flow rates along the downstream boundary for such a large number of outputs. This was tackled through the preparation of a macro code script, which enabled execution of repetitive multi-step tasks, without the need for individual processing. The macro code used for the processing of 599 simulation results is shown in Appendix A. For the calculation of t^*_{70} for each hydrograph obtained from Tecplot, the Matlab script explained in Section 2.5 was used.

4.3 Statistical analysis

In this study, the influence of 12 independent variables (11 shown in Figure 23 and ground roughness coefficient n) on the dependent variable t^*_{70} was considered, using results from 2,994 observations. This required the use of a statistical approach, chosen to be MLR, as it enables the study of each variable separately by isolating its role from all the others. The relationship between each independent and the dependent variable is determined from a linear approximation that best approximates the data points. This approach yields 12 regression coefficients, each representing the mean change in the dependent variable for one unit change in each independent variable, while holding other variables constant.

In order to enable a MLR approach, it is important to transform the 12 parameters into non-dimensional, scale invariant variables. Standardisation of each one of the 12 variables, named x_i where $i = 1, \ldots, 12$, was performed by subtracting the population mean μ_i from each variable x_i and then dividing by the standard deviation of the population σ_i. This was computed for the whole population of size $N = 2{,}994$, resulting in the following dimensionless quantity:

$$\overset{\frown}{x}_i = \frac{x_i - \mu_i}{\sigma_i} \tag{16}$$

Similarly, the dimensionless dependent variable t^*_{70} of mean μ and standard deviation σ for the population of size $N = 2{,}994$ was standardised into the form:

$$\overset{\frown}{t}_{70} = \frac{t_{70} - \mu}{\sigma} \tag{17}$$

The dependent and independent non-dimensional variables obtained can be arranged in a matrix form, for all of the 2,994 observations:

$$\mathbf{X} = \begin{bmatrix} \overset{\frown}{x}{}_1^{1} & \overset{\frown}{x}{}_2^{1} & \cdots & \overset{\frown}{x}{}_{12}^{1} \\ \overset{\frown}{x}{}_1^{2} & \overset{\frown}{x}{}_2^{2} & \cdots & \overset{\frown}{x}{}_{12}^{2} \\ \vdots & \vdots & \ddots & \vdots \\ \overset{\frown}{x}{}_1^{2,994} & \overset{\frown}{x}{}_2^{2,994} & \cdots & \overset{\frown}{x}{}_{12}^{2,994} \end{bmatrix} \quad \text{and} \quad \mathbf{T} = \begin{bmatrix} \overset{\frown}{t}{}_{70}^{1} \\ \overset{\frown}{t}{}_{70}^{2} \\ \vdots \\ \overset{\frown}{t}{}_{70}^{2,994} \end{bmatrix} \qquad (18), (19)$$

A multiple linear regression was then used to obtain the vector containing the coefficients β_i describing the assumed linear relationship for each parameter, using the least squares criterion:

$$\hat{\beta} = \left(\mathbf{X}^T\mathbf{X}\right)^{-1}\mathbf{X}^T\mathbf{T} = \begin{bmatrix} \beta_1 \\ \beta_2 \\ \vdots \\ \beta_{12} \end{bmatrix} \tag{20}$$

Coefficients β_i will then characterise the sensitivity of the non-dimensional time to each one of the 12 non-dimensional urban characteristics x_i.

4.4 Results and discussion

In this section, we first describe the results from the statistical approach and identify the most influential parameters on t^*_{70}. This is followed by an interpretation of the results and discussion on the most influential parameters. Finally, the relationship of the two most influential parameters with the dependent variable was visualised and discussed.

4.4.1 Regression coefficients

Table 3 and Figure 25 show the 12 coefficients β_i obtained from the regression analysis, representing the sensitivity factors on the dependent variable t^*_{70}. Positive coefficients indicate a positive correlation between the parameters and the dimensionless time and contrariwise for negative values. The ratio between each coefficient β_i and the largest coefficient β_{max} was also calculated to reveal the differences between the sensitivities of the parameters.

Overall, it can be concluded that the MLR model developed is very reliable as was shown by a zero associated p-value and $R^2 = 0.96$, very close to unity. A zero p-value indicates that the model, consisting of 12 independent variables, can reliably predict the dependent variable. In order to consider the reliability of each coefficient β_i to predict non-dimensional t^*_{70}, the p-value for each coefficient was determined. Each p-value tests the null hypothesis that the coefficient is not statistically significant. A low p-value (< 0.05) signifies that the null hypothesis can be rejected. All of the p-values were found to be near zero and < 0.05, confirming the statistical significance of each coefficient. Regarding R^2, a value of 0.96 indicates that 96% of the variance in the dependent variable can be predicted from the independent variables. Due to the high number of data points used in the analysis (2,994), the adjusted R^2, a more reliable indicator, was 0.96. This is also very close to unity, again confirming the reliability of the model.

Table 3. Regression coefficient for parameters P1-12

	Parameters	$\boldsymbol{\beta_i}$	$\boldsymbol{\beta_i / \beta_{max}}$
P1	Street length	0.0623	6.7%
P2	Street orientation	0.0127	1.4%
P3	Street curvature	0.0123	1.3%
P4	Street width (major)	-0.0064	-0.7%
P5	Street width (minor)	-0.0029	-0.3%
P6	Park coverage	-0.0111	-1.2%
P7	Parcel area	-0.0471	-5.0%
P8	Front setback	-0.0117	-1.3%
P9	Rear setback	0.0165	1.8%
P10	Side setback	-0.0427	-4.6%
P11	Building coverage	0.3160	33.8%
P12	Roughness n	**0.9346**	**100.0%**

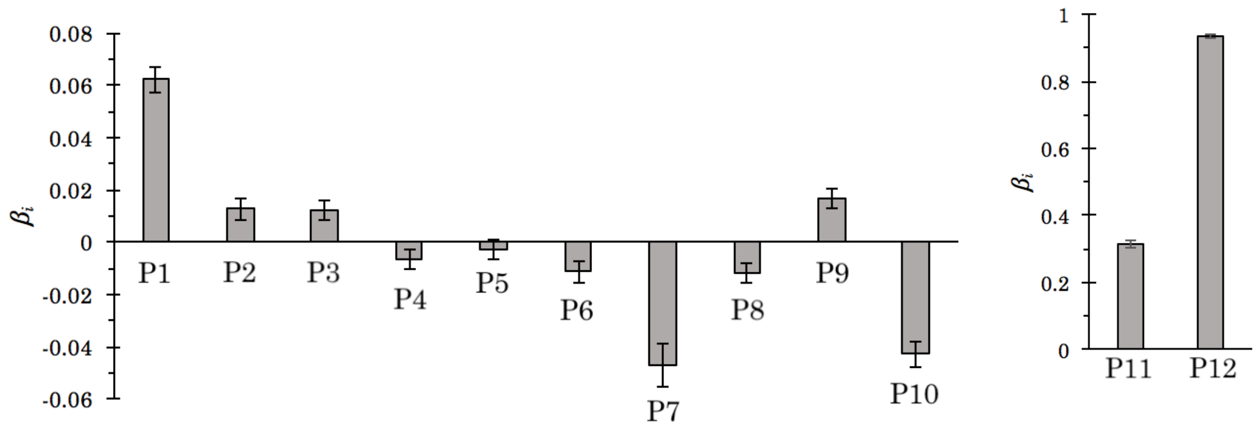

Figure 25. Graphical representation of 12 regression coefficients

As seen from Table 3 and Figure 25, the most influential parameter is roughness *n* (P12), followed by building coverage (P11). These two are many times more influential than the other parameters, which is why they were plotted in a separate scale. The large influence of roughness on dimensionless time can be explained by the low water depth developed during the rainfall events. In shallow water, it is expected that the flow is largely governed by microscale topography, rather than macroscale characteristics such as P1-11. As expected, building coverage was the second most influential parameter; flow of water is largely guided by the presence of buildings in the domain. Although it could be argued that an advantageous street network in a dense urban environment could in theory ease the flow of water out of the city, it is highly unlikely in randomly generated urban layouts. The same can be said for real-life urban environments which are designed and developed in a 'random' fashion, without any consideration for such aspects.

Street length (P1), which represents the average length of the streets present in the layout, also has a significant effect on the dimensionless time. One plausible explanation is the influence this parameter has on the overall geometry of the layout. Longer streets imply larger blocks of buildings, which in turn reduces the number of available flow paths. Water finds it easier to move around the building blocks and avoid the area inside blocks, hence a longer time to leave the urban area. The same can be said for building side setback P10; greater side gaps between buildings increase the number of available flow paths for water, hence the negative relationship with dimensionless time.

Parcel area (P7) is a measure of the area belonging to a single building. The individual effect of parcel area on water flow is therefore not easily explainable, since the building side, front and rear setback will also have a major contribution. It could be argued however, that generally, a large parcel area implies more space for water to flow. This would result in more possible flow paths and therefore lower dimensionless time. Front building setback (P8) contributes to the available are for water flow by 'widening' the width of the roads, hence the negative relationship with time. In the contrary, rear setback (P9) showed a positive relationship. This could be explained by the fact that an increasing back-to-back gap between buildings (as rear setback is increased) eases the accumulation of water in between building blocks. In this case, this could 'delay' the water as it moves towards the outlet.

The positive values for street orientation (P2) and curvature (P3) in some way related, as they 'guide' the flow of water. As expected, an increase in the curvature slows down the water, which 'prefers' straight flow paths, analogous to the natural flow of rivers. The effect of street orientation, on the other hand, is more complex since will be affected by the direction of the slope. In our case, slope direction was horizontal, which corresponds to a zero angle of orientation. This can also be seen in layout B of Figure 23, where a nearly horizontal street orientation has a street angle of 24^{o}. Therefore, it is expected that an increasing angle of orientation 'delays' the flow. This is confirmed by the positive relationship between P2 and dimensionless time.

The very low negative influence of the street width, both major (P4) and minor (P5), seems rather counter-intuitive at first sight. One can expect the water to find it much easier to move across an urban with very wide streets. However, the street geometry in urban environments is highly complex and it is more likely that water flow is influenced by a combination of other factors. These could in theory result in a very advantageous street network, which easily guides the flow of water out of a city, even though the streets are might not be as wide as expected.

4.4.2 Alternative models

Since roughness n dominates the response of the urban layout, a similar MLR approach will be performed by keeping n constant, reducing in this way the number of independent variables to 11. Since only three values of n (0.02, 0.04 and 0.07) were used for the 2,994 simulation results, using a single n value reduces the number of observations to 998. With a reduced number of observations, the reliability of the MLR model will be a concern. Therefore, three MLR models were developed separately, each using a different n. The regression coefficients for each model are compared in Figure 26.

Out of the three models, the one with n = 0.07 $m^{-1/3}s$ proved to be the most reliable, with the largest R^2 = 0.75 and lowest p-values for the 11 regression coefficients. Generally, the results obtained did not differ significantly from those shown in Figure 25, with the main differences being building coverage (P11) and parcel area (P7). The coefficients of both parameters appear to increase with an increase in roughness coefficient n. This is more evident for building coverage, suggesting the increasing influence of this parameter as flow is slowed down by increasing n. The order of influence among parameters remained the same as before, confirming the reliability of the MLR model with 12 variables and the conclusions resulting from it.

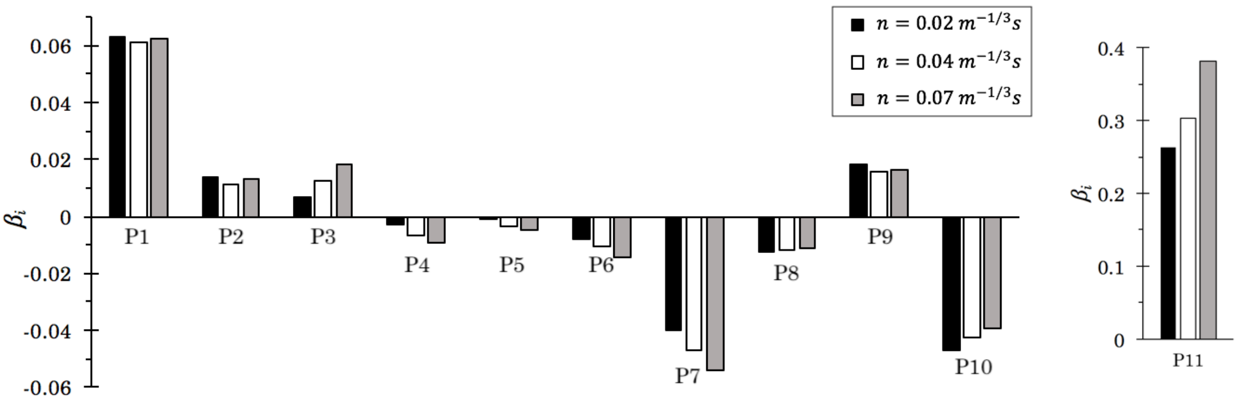

Figure 26. Graphical representation of 11 regression coefficients from three MLR models

4.4.3 Governing urban parameters

It was shown in Section 4.4.1 that t^*_{70} can be expressed as a linear function of β's (linear in parameters) as well as a linear function of x's (linear in variables). The MLR model developed with 12 variables displayed god fit to the data, confirming its statistical significance. In order to identify patterns, relationships or anomalies beyond the statistical results it is important to be able to visualise the results. However, visualisation of data in our case is rather challenging, since we are dealing

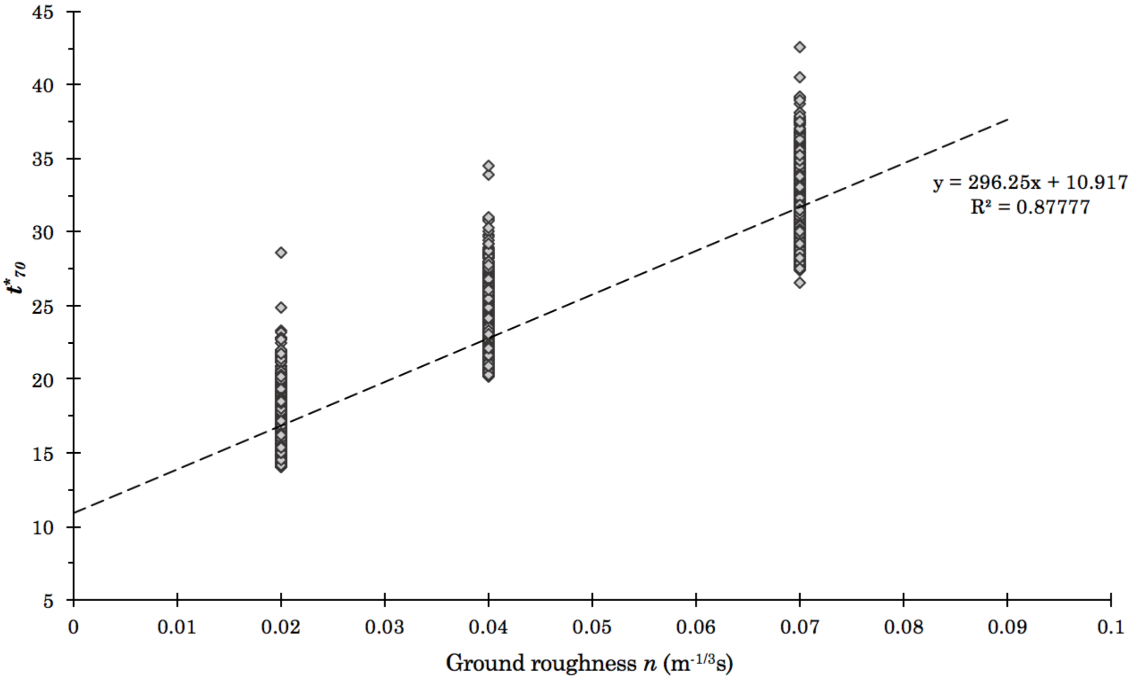

Figure 27. Linear fit of t^*_{70} vs. Manning roughness coefficient n

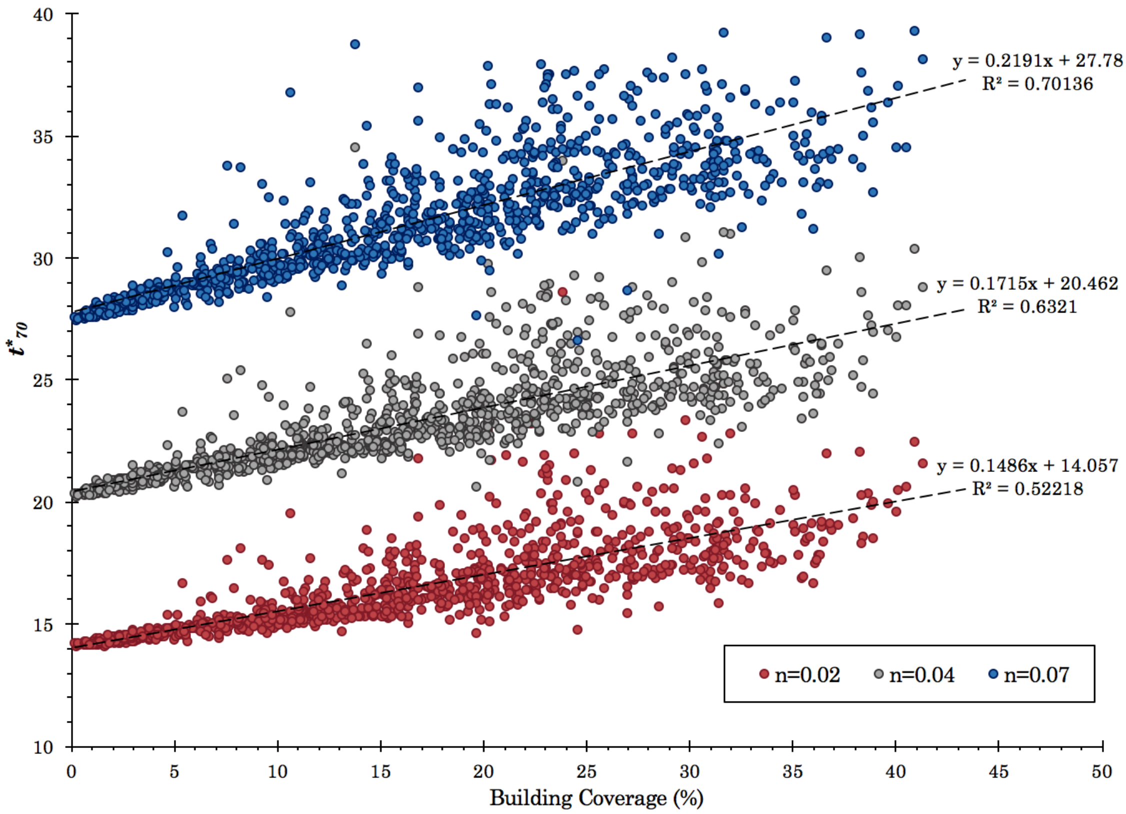

Figure 28. Linear fit of t^*_{70} vs. building coverage for all values of n

with a multi-dimensional model with 12 parameters. Use of pairs plot, also known as a scatterplot matrix, enabled visualisation of two-dimensional relationships between independent and standardised dependent variables. As expected, no visible relationship was observed for parameters P1-10 (shown in Appendix B) as the response of t^*_{70} is largely governed by n (P12) and building coverage (P11). Plotting t^*_{70} against these two parameters (non-standardised) in Figures 27-28 revealed the linear relationships derived from the statistical analysis. Although these relationships contain mixed information from other parameters P1-10, it can be argued that the presence of these parameters is governed by the building coverage.

From Figure 28, it can be seen that the data points collapse to a single line at low building coverages and eventually a single point at zero building coverage. At this point, the domain is simply a sloping plane of a roughness n without obstacles. The dimensionless time for water to leave the domain is thus simply governed by the roughness coefficient n. The lines of best fit to the data points belonging to different n values near zero building coverage are therefore distinct, clearly visible in Figure 28.

Increasing the building coverage, on the other hand, introduces additional variables affecting the flow of water. The influence of the other parameters (P1-10) on dimensionless time is therefore increasing with a growing building coverage, shown by an increasing deviation of data points in Figure 28. The data points belonging to different n values are not as distinct as before, suggesting the growing presence of other parameters. This can also be seen in Figure 27, with the increasing variation of t^*_{70} at different n's.

The change in n is also seen to affect the influence of building coverage on the dimensional time. The gradients of the lines of best fit in Figure 28 are increasing with an increasing n. This suggests an increasing influence of building coverage on t^*_{70}, also shown by the statistical analysis (Figure 26). For a reduction of ground roughness n to very low values, we expect t^*_{70} to become independent of building coverage.

4.4.4 Flow field observation

As shown in the previous sections, results for the dimensionless time t^*_{70} vary across a wide range of values and are largely governed by roughness coefficient n (P12) and building coverage (P11). Three computed urban layouts with the largest t^*_{70} values were examined in detail by visualising their flow fields and relating t^*_{70} with their respective urban parameters. All three layouts were chosen with the same ground roughness n = 0.04 $m^{-1/3}s$, in order to offer a better explanation of the influence of the other parameters. The flow fields for the three layouts named A-C are shown in Figure 29, with buildings shown in white and contours representing the magnitude of unit width flow rates.

Generally, the highest values of t^*_{70} belonged to urban layouts of large building coverage (P11), such as A and C. This was not the case for layout B, which has an intermediate building coverage (P11), suggesting t^*_{70} is largely influenced by other parameters. One such parameter is street length (P1), at 295 metres. It was suggested in Section 4.4.1 that longer streets imply larger blocks of buildings, which are largely avoided by water which finds it easier to bypass them. This can be confirmed by visualising the flow field of computed layout B. Contours of q inside the building blocks display low flow velocities, suggesting little contribution of this area to the flow of water. Flow is instead intensified along the streets, shown by the considerably higher flow velocities. Another effect of larger building blocks with low building setbacks is the accumulation of rainfall inside the blocks. This further slows down the flow of water, shown by the higher flow velocities in the narrow gaps between buildings. Street orientation (P2) is also highly disadvantageous in this case, with streets diverting the flow away from the slope direction, further delaying the time to reach the outlet.

In layout A, the low average street length (P1) allows for a better flow distribution around the domain. High velocities are only developed near the outlet, at narrow contractions and crossroads. Furthermore, street orientation is advantageous, aligning the flow in the slope direction. Nevertheless, flow is largely governed by the dense building network and high street curvatures (P3) which divert the flow away from a straight, short path. These two factors govern the response, resulting in the high dimensionless time.

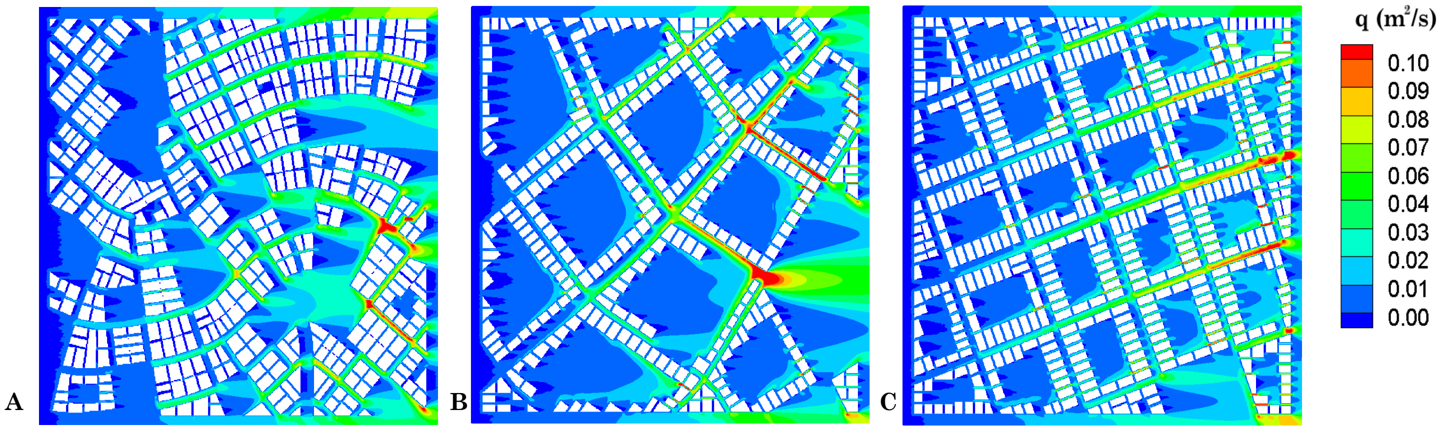

	P1	P2	P3	P4	P5	P6	P7	P8	P9	P10	P11	t^*_{70}
A	100.5m	57.3°	0.341	29.9m	12.4m	26.3%	1073m^2	1.0m	1.1m	2.8m	37.2%	**26.5**
B	295.0m	155.1°	0.287	28.5m	10.3m	23.7%	898m^2	1.1m	3.0m	3.0m	23.2%	**28.9**
C	212.3m	24.0°	0.051	20.7m	12.8m	10.4%	810m^2	1.1m	1.9m	3.1m	34.4%	**27.1**

Figure 29. Flow fields and urban parameters for three configurations of highest t^*_{70} values (n = 0.04 $m^{-1/3}s$)

Similarly, flow in layout C is mainly governed by building coverage (P11). Furthermore, the relatively large street lengths (P1) and low building setbacks (P8-P10) create ‘void’ areas between building blocks with negligible flow, causing a similar effect as in layout B. There is however, negligible street curvature and better flow distribution. This increases the number of available flow paths for water, hence the lower t^*_{70}, despite having a greater building coverage than layout B.

4.4.5 Implication for urban planning

Flood-resilient urban design implies fast conveyance of surface runoff to storage areas and prevention of its accumulation inside urban environments. As was shown in the previous sections, this is equivalent to reducing the dimensionless time t^*_{70}, which can be achieved by careful control of the urban parameters affecting it.

The most influential factor was shown to be Manning roughness coefficient n; lowering n would have a positive contribution in the efficient conveyance of flood water. In urban areas, this can be achieved through an increase in paved surfaces, which have the lowest n coefficients. This, however, has a negative effect in the amount of infiltrated water from rainfall, as paved surfaces are highly impermeable and encourage accumulation of water over the ground. Therefore, a reduction in the infiltration zones is not desired; a lower roughness coefficient n can be achieved through removal of obstacles/barriers and smoothening of surfaces in existing impervious surfaces.

Building coverage was found to be the second most influential factor. Dense built environments delay the flow of runoff by reducing the surface area available for water flow. Another consequence is the significant increase in water depths, which cause devastating effects during flash floods. Therefore, design of future flood-resilient urban areas can be achieved by imposing upper limits on building coverage. An alternative approach is an advantageous combination of street orientation and building side setback, which can effectively compensate for a high building coverage, shown to be the case for layout A (Figure 29).

It was shown in the previous sections that an advantageous street orientation and small curvatures can reduce the time for runoff discharge. In the context of urban planning, this can be achieved through proper design of street networks. Straight, short streets, aligned along slope directions, will guide the flow efficiently towards the outlet. Shorter streets imply larger building blocks, which in turn increase the size of 'void' surface areas not contributing to surface flow. This can be seen in Figure 30, where very low flow velocities (represented by contours and vectors) are observed inside the building blocks.

Another influential parameter is building side setback, which effectively controls the side gaps between buildings. Wider gaps increase the number of available flow paths for water, contributing in this way to the reduction of void areas between building blocks, also seen in Figure 31.

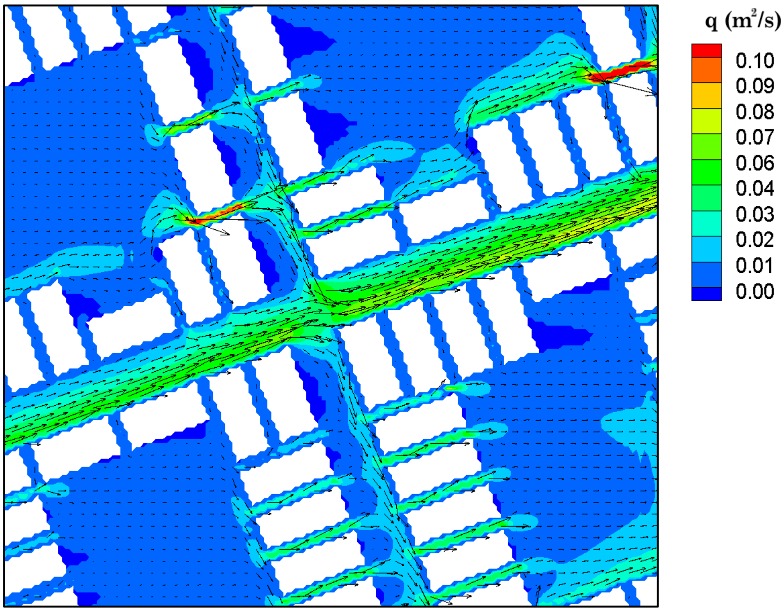

Figure 30. Void areas inside building blocks

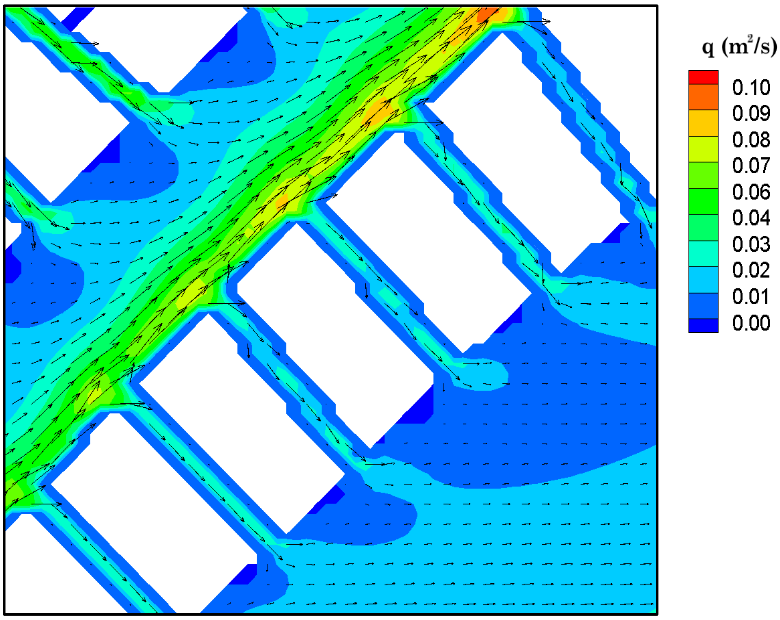

Figure 31. Flow field through gaps between buildings

5 Conclusions

In the first stage of the project, the hydrodynamical model was successfully validated against published results. General agreement with results from Bruwier *et al.* (2017) confirmed the capability of the model in simulating prescribed water flow over realistic urban layouts. Successful validation was also attained against a kinematic model, confirming our model can correctly predict overland flow over impermeable sloping planes under uniform, constant rainfall of a finite duration. Re-examination of the S-curve normalisation theory for realistic urban layouts showed that dimensionless hydrographs using a properly-constructed dimensionless time under different combinations of catchment and rainfall parameters collapse to a single curve. This confirms that the derived dimensionless S-curve is only a function of urban characteristics, allowing the use of a dimensionless time, t^*_{70} to characterise the rainfall-runoff response.

The S-curve normalisation theory paved the way for the final stage of the project, a parametric urban runoff study. High performance computing, parallel processing and automation enabled the simulation and processing of 2,994 rainfall-runoff processes. Analysis of the results was achieved through the development of a reliable multiple linear regression model, which quantified the sensitivity of t^*_{70} to 12 urban characteristics. It was shown the most influential factors are Manning roughness coefficient n and building coverage. Less influential were found to be street length, building side setback, parcel area and to a lesser extent, street orientation and curvature. The order of influence among parameters remained the same when three additional models with 11 parameters were developed, by keeping the 12$^{\text{th}}$ parameter n constant. Visualising flow fields for three computed urban layouts with the highest t^*_{70} revealed that conveyance is highly influenced by building coverage, street length and building side setback, re-confirming the regression results.

Careful investigation of the relationships between t^*_{70} and the two most influential parameters, building coverage and roughness, revealed that influence of building coverage on t^*_{70} is reduced at low n values. For a very smooth ground surface, of very low n, we expect t^*_{70} to eventually become independent of building coverage. Also, the variation in t^*_{70} decreased at low building coverages, converging to a single point at zero building coverage where flow is only affected by n. This suggests a decreasing influence of other urban characteristics as building coverage gets closer to zero. This is expected, since the absence of buildings in the domain implies the absence of other urban parameters, hence their influence on t^*_{70}.

Flood-resilient urban design implies fast conveyance of surface runoff to storage areas, which can be achieved by reducing the dimensionless time t^*_{70}. Potential measures include removal of obstacles/debris in existing paved surfaces to reduce n or imposing limits on the allowable building coverage. A similar effect can be achieved by proper design of street networks; shorter roads aligned along the slope direction, combined with wider gaps between buildings were all shown to improve conveyance by increasing the available area for water flow.

Rainfall-runoff processes in urban environments are highly complex, as was shown to be influenced by multiple factors. This project decoupled these factors and quantified their influence on the hydrological response of urban areas, providing valuable knowledge on the influence of urban characteristics on rainfall-runoff processes. This paves the way for more parametric studies of this kind that can provide more insight on the design of future flood-resilient built environments.

Urban environments contain additional features such as roads, parks and drainage infrastructure, which are not considered in our model. Further research is required to investigate the influence of features such as terrain infiltration and drainage rates as well as the outflow boundary conditions and their effect on the response of the catchment. Additionally, the assumption of a generalised ground roughness coefficient and its implications on the catchment could be further investigated.

6 References

Bazin, P.-H. (2013). Flows during floods in urban areas: Influence of the detailed topography and exchanges with the sewer system. University Claude Bernard - Lyon I.

Bruwier, M., Mustafa, A., Aliaga, D. et al. (2017). Influence of urban patterns on flooding. *Proceedings of the 37th IAHR World Congress*.

Cea, L., Garrido, M. et al. (2009). Experimental validation of two-dimensional depth-averaged models for forecasting rainfall-runoff from precipitation data in urban areas. *Journal of Hydrology*, 382(1-4), 88–102.

Chan Y. (2012). Rainfall-runoff processes in urban environments. MEng Final Report. University of Cambridge.

Douglas, I., S. Garvin, N. Lawson. et al. (2010). Urban Pluvial Flooding: A Qualitative Case Study of Cause, Effect and Non-structural Mitigation. *Journal of Flood Risk Management* 3 (2): 112–125.

Environment Agency (2007). Review of 2007 summer floods. Bristol: *Environment Agency*, pp. 15.

Environment Agency (2009). Flooding in England: A National Assessment of Flood Risk. Bristol: *Environment Agency*, pp. 6-8.

Henderson, F. & Wooding, R. (1964). Overland flow and groundwater flow from a steady rainfall of finite duration. *Journal of Geophysical Research* Vol. 69, No.8.

Huang, C.-J., M.-H. Hsu, W.-H. Teng, and Y.-H. Wang. (2014). The impact of building coverage in the metropolitan area on the flow calculation. *Water* (Switzerland) 6:2449–2466.

Jenkins, G.J., Perry, M.C., and Prior, M.J. (2008). The climate of the United Kingdom and recent trends. Met Office Hadley Centre, Exeter, UK.

Lam P. (2016). Rainfall-runoff processes in urban environments. MEng Final Report. University of Cambridge.

Liang, D., Lin, B., & Falconer, R. (2006). Simulation of rapidly varying flow using an efficient TVD–MacCormack scheme. *International Journal for Numerical Methods in Fluids*, pp. 811-826.

Liang, D., Özgen, I., Hinkelmann, R. et al. (2015). Shallow water simulation of overland flows in idealised catchments. *Environmental Earth Sciences* 74: 7307.

Liew Z. (2017). Rainfall-runoff processes in urban environments. MEng Final Report. University of Cambridge.

Mignot, E., A. Paquier, and S. Haider (2006). Modelling floods in a dense urban area using 2D shallow water equations. *Journal of Hydrology* 327:186–199.

Overton, D. & Brakensiek, D. (1970). A kinematic model of surface runoff response. *Proceedings of Symposium Results of Research on Representative and Experimental Basins*, Wellington, New Zealand.

Özgen, I., Liang, D and Hinkelmann, R (2016). Shallow water equations with depth-dependent anisotropic porosity for subgrid-scale topography. *Applied Mathematical Modelling*, 40. pp. 7447-7473.

United Nations, Department of Economic and Social Affairs, Population Division (2015). World Population Prospects: The 2015 Revision, Key Findings and Advance Tables.

7 Appendices

7.1 Appendix A: Tecplot automation macro code

```
#!MC 1410

$!Loop 599

 $!VarSet |loop1| = (|loop|+400)
 $!VarSet |MFBD| = 'C:\Program Files\Tecplot'
 $!DRAWGRAPHICS FALSE
 $!READDATASET  '"\\Mac\Home\Desktop\buildings_000|loop1|_UVE.DAT" '
  READDATAOPTION = NEW
  RESETSTYLE = YES
  VARLOADMODE = BYNAME
  ASSIGNSTRANDIDS = YES
  VARNAMELIST = '"X" "Y" "ZB" "E" "QX" "QY" "IWET"'

 $!PLOTTYPE = CARTESIAN2D
 $!EXTENDEDCOMMAND
  COMMANDPROCESSORID = 'CFDAnalyzer4'
  COMMAND = 'Integrate [1-42] VariableOption=\'Scalar\' XOrigin=0
YOrigin=0  ZOrigin=0  ScalarVar=5 Absolute=\'F\'
ExcludeBlanked=\'F\' XVariable=1 YVariable=2 ZVariable=3
IntegrateOver=\'Cells\' IntegrateBy=\'Zones\' IRange={MIN =1 MAX = 0
SKIP = 1} JRange={MIN =1 MAX = 0 SKIP = 1} KRange={MIN =1 MAX = 0
SKIP = 1} PlotResults=\'F\' PlotAs=\'Result\' TimeMin=0 TimeMax=0'

 $!EXTENDEDCOMMAND
  COMMANDPROCESSORID = 'CFDAnalyzer4'
  COMMAND = 'SaveIntegrationResults
FileName=\'\\\\Mac\\Home\\Desktop\\buildings_000|loop1|.txt\''

$!EndLoop


$!RemoveVar |MFBD|
```

7.2 Appendix B: Pair plots of standardised parameters

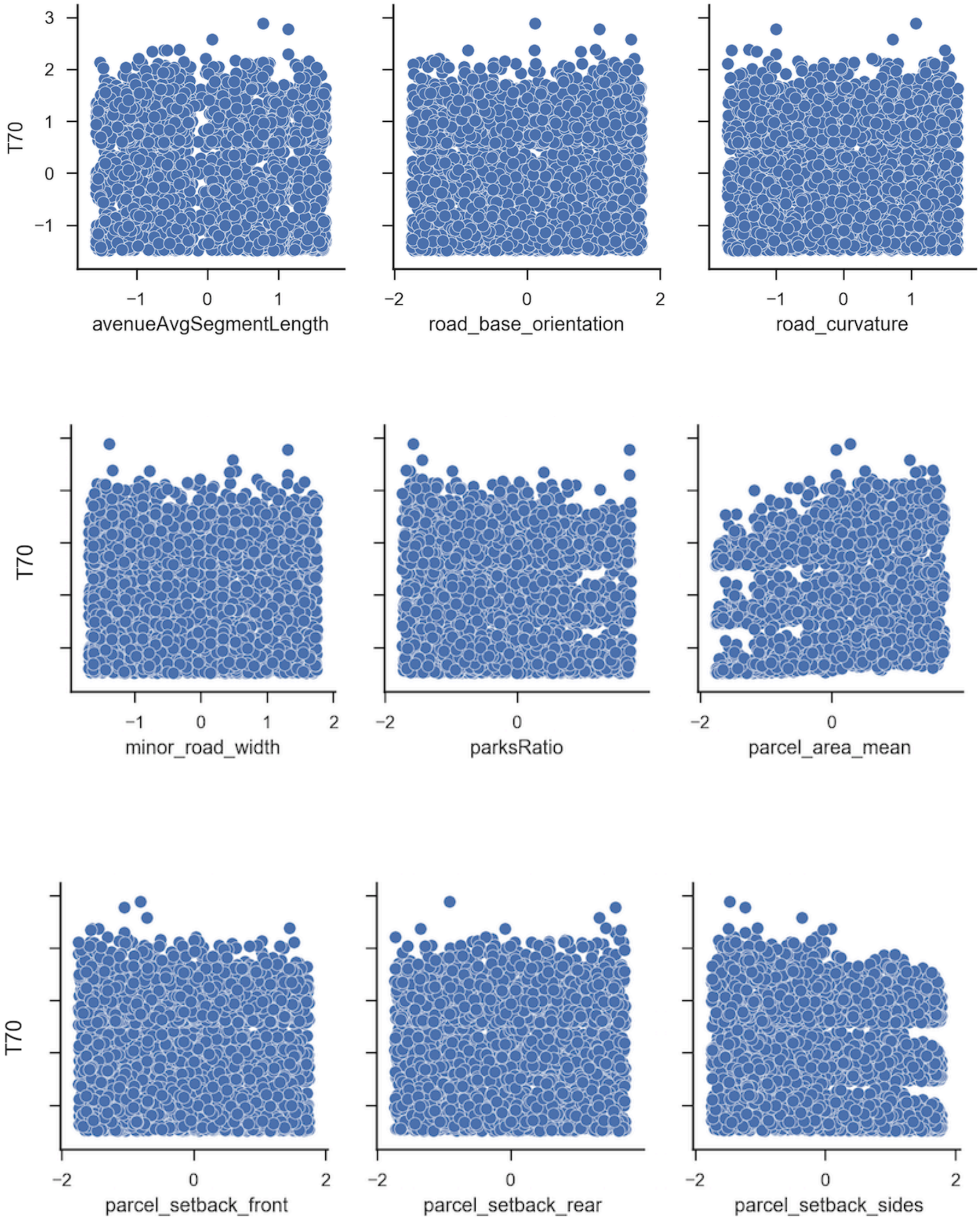

Figure 32a-i. t^*_{70} vs. standardised parameters P1-9

7.3 Appendix C: Risk assessment retrospective

The major risks associated with this project were the health risks caused by prolonged use of computers and lack of physical activity. These included musculoskeletal problems arising from incorrect posture and eyestrain from prolonged eye focusing on computer screens. The risks became more evident as deadlines approached, also due to lack of physical activity.

Attempts were made to avoid exposure to computers while waiting for computational simulations and maximise physical activity where possible. These became more prominent as the year progressed with the introduction of short, frequent breaks as well as regular physical and eye exercises. In retrospect, the risks mentioned above are highly pertinent and can be easily overlooked. Therefore, more caution should be exercised with these risks when working on such projects in the future.